Multiplicative or t_1 Noise in NMR Spectroscopy

Josef Granwehr[1]

Materials Sciences Division

Lawrence Berkeley National Laboratory

1 Cyclotron Road

Berkeley CA, 94720

and

Department of Chemistry, D-62 Hildebrand Hall

University of California

Berkeley CA, 94720

Phone: (510) 642-7717

Fax: (510) 486-5744

10th April 2006

[1]e-mail: joga@waugh.cchem.berkeley.edu

ABSTRACT

The signal in an NMR experiment is highly sensitive to fluctuations of the environment of the sample. If, for example, the static magnetic field B_0, the amplitude and phase of radio frequency (rf) pulses, or the resonant frequency of the detection circuit are not perfectly stable and reproducible, the magnetic moment of the spins is altered and becomes a noisy quantity itself. This kind of noise not only depends on the presence of a signal, it is in fact proportional to it. Since all the spins at a particular location in a sample experience the same environment at any given time, this noise primarily affects the reproducibility of an experiment, which is mainly of importance in the indirect dimensions of a multidimensional experiment, when intense lines are suppressed with a phase cycle, or for difference spectroscopy techniques. Equivalently, experiments which are known to be problematic with regard to their reproducibility, like flow experiments or experiments with a mobile target, tend to be affected stronger by multiplicative noise. In this article it is demonstrated how multiplicative noise can be identified and characterized using very simple, repetitive experiments. An error estimation approach is developed to give an intuitive, yet quantitative understanding of its properties. The consequences for multidimensional NMR experiments are outlined, implications for data analysis are shown, and strategies for the optimization of experiments are summarized.

KEY WORDS: NMR; sensitivity; multiplicative noise; t_1 noise; field–frequency lock; remote detection; flow

INTRODUCTION

For a quantitative sensitivity analysis in NMR, the distinction between additive and multiplicative noise must be made. Additive noise is either generated by the detector and any subsequent devices, which is the dominant source in high-field NMR [1, 2, 3], or induced by an external source with a significant spectral density in the same frequency band as the signal, which is mainly of importance at low magnetic fields [4]. Its noise power does not depend on the amplitude of the signal. Thermal white electronic noise (Johnson noise) from the detection circuit is usually considered the main additive noise source. It is a fundamental quantity of inductive detectors whose characterization is reasonably straightforward [5], even with lossy samples like in medical imaging [6]. In contrast, environmental influences on the sample magnetization like instrumental instabilities or fluctuating external electromagnetic fields as well as the reproducibility of rf pulses affect the signal or the signal-inducing quantity [7, 8]. This type of noise is multiplicative as it grows with the signal and is often proportional to it. Because in NMR spectra its impact is obvious primarily along the indirect dimensions of multidimensional experiments, it is often referred to as t_1 noise. For example, a small change in pulse amplitude or phase between different traces in a two-dimensional (2D) experiment leads to a slight variation of the signal that is proportional to the affected spin magnetization [9, 10]. This effect goes almost unnoticed in the transiently detected direct (or t_2) dimension, because it leads to a systematic error that is identical for all affected spins. The situation changes for an interferogram that is recorded point-by-point along an indirect dimension [11]. Fluctuations of the signal are uncorrelated for independent points or traces and appear as white noise, leading to ridges proportional to the signal intensity along this indirect dimension. Since such imperfections significantly reduce the reproducibility of an experiment, they cause noise not only in the indirect dimensions of multi-dimensional experiments or in experiments with point-by-point acquisition, but also in one-dimensional (1D) experiments with transient detection where part of the signal is subtracted, like in NOE difference spectroscopy [12] or if a phase cycle is used to remove certain coherences.

Sources for multiplicative noise can be manifold [7]. During free precession of transverse spin magnetization, an important source is a fluctuating static magnetic field B_0. The origin of such fluctuations could be instabilities of the magnet itself, for example caused by floor vibrations or by the adjusting of the dewar

to an altered thermal environment after a magnet refill [13]. Thermoacoustic oscillations [14] have been suggested in this context as well. Noisy shim coils and shim power supplies could be a source of spatially dependent B_0 fluctuations. The same applies to field gradient coils if present. Furthermore B_0 noise can be induced when a noisy external magnetic field is coupled inductively with the magnet that generates the main B_0 field. This is serious for unshielded as well as for shielded magnets, where the shielding coil is in series with the main coil. While the field outside the magnet is canceled by the shield, the field in the bore is not, therefore it is still possible to couple noise from the outside of a magnet into the bore. Sources could be, for example, electronic devices in the vicinity of the magnet, an elevator that induces a regular pattern but at random times, or the opening of a door to the room with the magnet. During rf irradiation, additional noise contributors become important [8, 15, 16] like instabilities of the rf frequency and amplitude as well as jitter, caused by frequency synthesizers and high-power rf amplifiers. Depending on the setup and its environment, mechanical vibrations can be another noise source of importance with manifold consequences. They can originate from not rigidly mounted parts of the probe, which then are moved for example by air flowing through the probe for temperature controlling, or they can stem from small vibrations of the floor. This alters the properties of the rf circuit like its quality factor Q or the tuning and matching. A quantitative discussion can be done by analyzing the change these vibrations induce in the transfer function of the detection circuit, which requires a thorough understanding of the mechanical and the electronic properties of the magnet and the probe [17, 18].

Temperature fluctuations of the sample or parts of the electronic circuit in the probe may be another potential source of multiplicative noise [19]. If the temperature changes are primarily caused by the interaction with electromagnetic radiation from the rf pulse, this may be considered a source of systematic errors. But the chemical shift of some samples is strongly temperature dependent [20], so that even fluctuations of a few milli-kelvin cause an observable effect. Note that a temperature dependent resonance frequency of the nucleus used for field–frequency locking would have an equivalent impact on the result.

NMR and magnetic resonance imaging with flowing fluids is especially prone to multiplicative noise. Fluctuations of the flow rate is the most apparent source, but depending on the setup, other causes could be vibrations of the flow tubing or devices induced by the fluid, and a change of the sample impedance and therefore the tuning and matching of the detection circuit if bubbles are present in a liquid or if the pressure

of a gas is not stable. The impact of flow rate fluctuations depends on the experiment that is performed and is especially severe when flow is studied on a long timescale. One such experiment is time-of-flight (TOF) remote detection NMR [21], where the spins of a fluid are tagged in an encoding environment and detected as the fluid leaves the porous object of interest using a second coil.

Clearly, the different multiplicative noise sources have vastly different noise spectral densities. While thermal electronic noise is Gaussian white noise up to the highest accessible NMR frequencies, perturbations that affect the stability of NMR spectrometers are generally not white. AC powered devices commonly show coherent noise at harmonics of the line frequency, *i.e.* multiples of 50/60 Hz. The magnetic noise at low frequencies in a laboratory environment tends to have a power spectrum that falls off with $1/f$, f being the frequency of each spectral component. Mechanical vibrations are typically at very low frequencies of a few Hertz or even sub-Hertz. Temperature fluctuations usually have a strong drift component, potentially mixed with the feedback characteristics of the temperature controller. And finally, the response of the field–frequency lock depends on the specific implementation in a particular spectrometer.

There are other errors of instrumental origin, which are of more systematic nature. The most prominent is probably radiation damping [22]. Eddy currents [23] can be important especially in experiments using pulsed field gradients, and errors due to a limited dynamic range of an rf preamplifier or due to the digitization of the signal can lead to line distortions or digital noise. These kinds of systematic errors will not be discussed here. Also errors related to or amplified by radiation damping like spin noise [24] or spin turbulence [25] will not be treated.

In this paper, it is demonstrated how the difference of the noise behavior between the transiently detected direct dimension and the indirect dimension of multidimensional NMR experiments can be understood quantitatively on the basis of a simple error estimation. A generic procedure is described and illustrated theoretically and experimentally on some simple model systems. The impact of a noisy environment is analyzed first in the time domain, and then it is shown how spectra are affected after Fourier transform (FT) of the measured interferogram. Furthermore, it is shown that the unequal behavior of noise in the direct and the indirect dimensions have important consequences for the design and performance of multidimensional NMR experiments. Some common causes for multiplicative noise and their effect on the signal are summarized. These include fluctuations of B_0, instabilities of the pulse phase and amplitude, mechanical vibrations, and

inheritance of noise if the spin magnetization does not fully relax to its equilibrium value between different repetitions of an experiment. The transient behavior of the noise often allows to identify its primary source, which then enables to quantify the noise inducing process itself. This is shown for fluctuations of the fluid flow rate in an experiment with remote detection. In this case it was not necessary to know an exact expression for the fluid dispersion between encoding and detection or to apply a curve fitting to the experimental data. It was sufficient to know the mean TOF pattern from a series of identical experiments and the standard deviation of the signal at each point of this pattern to find the standard deviation of the flow rate.

QUANTIFICATION OF SENSITIVITY

Additive noise depends on the detector and can be characterized without assuming anything about the signal – it is in fact easier to characterize in the absence of any signal. Multiplicative noise is imposed on the detected signal and therefore depends on the interaction of the signal-inducing quantity with the environment and with the detector. To discuss multiplicative noise quantitatively, it is necessary to model the signal such that it shows the correct dependence on environmental parameters. If the multiplicative noise amplitude is small compared to the signal, its variance σ_M^2 can be approximated by a first-order Taylor expansion of the noisy signal $s'(t, x_1, \ldots, x_m, \ldots, x_p)$ around the noiseless signal $s(t)$. If the noise-relevant quantities x_m, each with its own variance σ_m^2, are statistically independent, they add as

$$\sigma_M(t)^2 = \sum_{m=1}^{p} \left(\left. \frac{\partial s'(t, x_1, \ldots, x_m, \ldots, x_p)}{\partial x_m} \right|_{s(t)} \right)^2 \sigma_m^2 \,. \tag{1}$$

x_m represents any parameter, like B_0, or event, like an rf pulse, with an influence on the detected signal. In a noiseless environment x_m is constant, therefore it is not listed as independent parameter in the following equations.

With inductive detection, the time-domain signal $s(t)$ is proportional to the time derivative of the transverse magnetization $M^+(t)$, which for our purposes shall be given by [26]

$$M^+(t) = \sum_{k=1}^{N} M_k^+(t) = M_0 \sum_{k=1}^{N} A_k \, \exp\left(-t/T_{2,k} - i\gamma_k B_0 t\right) \,, \tag{2}$$

where N is the number of oscillators, M_0 is the equilibrium polarization of the sample, A_k is the relative

complex amplitude of each signal component k, $T_{2,k}$ is the decoherence time of each oscillator, and $\gamma_k = \gamma(1-\varsigma_k)$ with the gyromagnetic ratio γ and the chemical shift ς_k of each nucleus.

The induced signal depends on the equation of motion of the detection circuit. A model system is an LCR circuit, which can be described as a damped harmonic oscillator where the signal is a forced oscillation induced by the changing flux of the precessing $M^+(t)$. A rigorous treatment of multiplicative noise has to be done in the laboratory frame with the full consideration of the equation of motion of the detector [27]. However, because in high-field NMR the detected transients and mostly even the dwell time Δt between adjacent data points are considerably longer than the time constant of the detection circuit, and due to the large difference of several orders of magnitude between the spectral components of the multiplicative noise and the NMR frequencies, which are detected with a narrow bandwidth, the detector can be described by its steady-state solution. Its properties do not have to be taken into account when discussing noise of the signal-inducing quantity, and fluctuations of the detector properties can be discussed as fluctuations of its steady-state solution. This allows separation of the discussion of fluctuations of the spin magnetization and fluctuations of the detector properties. A simplified model for the signal can be used where constants and instrumental factors are neglected. Thus we define

$$s_k(t) = \frac{\partial M_k^+(t)}{\partial t} \approx -i\gamma_k B_0 \, M_k^+(t)\,, \tag{3}$$

and

$$s(t) = \sum_{k=1}^{N} s_k(t)\,. \tag{4}$$

We can describe each of the noisy signal transients as

$$s'(t) = s(t) + n(t)\,, \tag{5}$$

where $n(t)$ is the noise emf of each individual data point. It contains contributions from additive noise $n_+(t)$ as well as multiplicative noise $n_M(t)$. The variance as a function of the evolution time t can be calculated for N_S independent experiments as

$$\sigma_S(t)^2 = \frac{1}{N_s} \sum_{r=1}^{N_s} |s'_r(t) - s(t)|^2 = \langle |n(t)|^2 \rangle\,. \tag{6}$$

Deviations of $s'(t)$ from $s(t)$ can be caused not only by random noise, but also by drifts that are of systematic origin. Sometimes such drifts cannot be identified before the experiment is finished. To suppress their

influence, the data can be analyzed in differential form. Assuming that N_s is even, we can calculate

$$\begin{aligned}\frac{1}{N_s}\sum_{r=1}^{N_s/2}\left|s'_{2r}(t)-s'_{2r-1}(t)\right|^2 &= \frac{1}{N_s}\sum_{r=1}^{N_s/2}|n_{2r}(t)|^2+|n_{2r-1}(t)|^2-n_{2r}(t)n_{2r-1}(t)^*-n_{2r-1}(t)n_{2r}(t)^* \\ &\approx \frac{1}{N_s}\sum_{r=1}^{N_s}|n_r(t)|^2=\sigma_S(t)^2\,. \end{aligned} \tag{7}$$

If a drift contribution $a_d r$ as a function of the experiment number r with slope a_d is added to $s'(t)$, it adds an additional contribution of approximately $a_d^2 N_s^2/12$ to σ^2 if calculated according to Eq. (6), but only $a_d^2/2$ if σ^2 is calculated according to Eq. (7).

To specify the signal-to-noise ratio (SNR), which is a dimensionless quantity used to characterize the sensitivity of an experiment, it is necessary to distinguish between the time and the frequency domain. Usually, as detailed in [2], the SNR is defined in the frequency domain as the ratio of the on-resonant amplitude $|S(0)|$ of a reference signal to twice the root mean square (rms) noise amplitude, $\tilde{\sigma}_S(\Delta\omega)$. The factor 2 will be disregarded in the following, thus

$$(\mathrm{SNR})_\omega = \frac{|S(0)|}{\tilde{\sigma}_S(\Delta\omega)}\,. \tag{8}$$

The tilde is used to denominate σ in the frequency domain. $\tilde{\sigma}_S(\Delta\omega)$ contains contributions from additive noise, $\tilde{\sigma}_+$, and multiplicative noise, $\tilde{\sigma}_M(\Delta\omega)$. $\tilde{\sigma}_+$ is frequency independent, while $\tilde{\sigma}_M(\Delta\omega)$ depends on the offset $\Delta\omega$ from the center of the peak. In the time domain, it is for our purposes more useful to define the SNR using the signal from each individual data point,

$$(\mathrm{SNR})_t = \frac{|s(t)|}{\sigma_S(t)}\,. \tag{9}$$

If we assume that the signal in Eq. (1) does not influence x_m, then σ_M is proportional to M_0 times the decay function of the signal. Therefore one can define a signal-independent multiplicative SNR, ψ_M, which marks an upper limit for the sensitivity of a particular data point. In the time domain,

$$\psi_M(t) = \frac{|s(t)|}{\sigma_M(t)}\,, \tag{10}$$

and in the frequency domain,

$$\tilde{\psi}_M(\Delta\omega) = \frac{|S(0)|}{\sigma_M(\Delta\omega)}\,. \tag{11}$$

If multiplicative noise is due to several independent noise processes, each with its own ψ_m, they add up as

$$\psi_M = \left(\sum_m \psi_m^{-2}\right)^{-1/2}\,. \tag{12}$$

Since during an NMR experiment the signal intensity changes, for example due to relaxation, it is sometimes clearer to discuss multiplicative noise in terms of ψ_M than by a σ_M value. The SNR as a function of the signal amplitude for an experiment with both additive and multiplicative noise contributions is shown in Fig. 1. If the signal level is low, the SNR is dominated by additive noise and thus proportional to the signal. With increasing signal, the SNR approaches its maximum specified by multiplicative noise.

The simplest experiment to characterize multiplicative noise is to do several repetitions of a free induction decay (FID) after a single non-selective rf pulse using a sample with a large signal that has only few, well-separated lines. The size of this data set must be large enough to give a statistically significant statement about the noise-inducing process. Since every aspect of such an experiment can be controlled, it is important to suppress any effects that could lead to an increased noise level or that might complicate the assignment of the noise sources like radiation damping, dipolar demagnetizing field effects [28] of the solvent, heating of the sample, or memory effects between subsequent repetitions.

Two different spectrometers were used for the experiments presented here. One of them was a Unity Inova spectrometer (Varian Inc., Palo Alto CA) with an unshielded 7.05 T widebore magnet (Oxford Instruments, Cambridge UK), which corresponds to a proton frequency of 300 MHz. The other spectrometer was an Avance 700 (Bruker GmbH, Rheinstetten, Germany) with a shielded 16.4 T magnet (Bruker AG, Fällanden, Switzerland), having a proton frequency of 700 MHz. Both spectrometers were equipped with two-channel 5 mm liquids probes (one proton and one broadband channel, with a separate channel for the deuterium lock) from the respective manufacturer of the spectrometer. No experiments were done within one day after a magnet refill with cryogenics to allow the liquids to settle and the temperature within the dewar to stabilize.

NOISE AFFECTING THE SPIN MAGNETIZATION

Free Precession in a Static Magnetic Field

In high-resolution NMR experiments transverse magnetization $M^+(t)$ is precessing with a frequency of up to several hundred MHz, while spectral resolutions of a few Hz are obtained routinely. This requires a detection time of a single transient on the order of a second, and fluctuations of B_0 up to ten orders of magnitude smaller than B_0 itself can have a noticeable influence on the phase of $M^+(t)$. Such phase errors

can be converted into amplitude errors for example by a pulse, which affects only one component of the transverse magnetization, by co-adding several experiments, or by phasing the signal and retaining only its real component.

A quantitative discussion of the error accumulating during free evolution in a noisy B_0 field can be done with either t or B_0 as the independent parameter. The first part of the discussion will be done with B_0 as the independent parameter, which is more intuitive, but does not give an estimate of the noise over time scales longer than the correlation time, τ_B, of the B_0 noise. A more general discussion will be made about the long-time behavior of the noise with t as the independent parameter. More formal solutions to determine the SNR during a transient evolution of the spin magnetization due to phase noise can be found in the literature [27, 29] by noting the similarity of this problem to the characterization of a complex oscillator with noisy frequency.

The noise during the FID due to fluctuations of B_0 can be approximated as

$$n_B(t) = B_n \frac{\partial s(t)}{\partial B_0} \approx -B_n M_0 \sum_{k=1}^{N} A_k \gamma_k^2 B_0 t \, \exp\left(-\frac{t}{T_{2,k}} - i\gamma_k B_0 t\right) = -iB_n t \sum_{k=1}^{N} \gamma_k s_k(t)\,, \tag{13}$$

where B_n is the deviation of B_0 from its mean value. For now, B_n is assumed to be constant during each repetition of the experiment. The noise is proportional to the sum of all the signals from the different lines because each signal component sees the same B_0. Note that the dominant part of the noise is phase shifted by 90° compared to the signal. Therefore the real part of the signal determines the noise of the imaginary part and vice versa, which is characteristic for a phase error – if the cosine component of a signal is at its maximum, a small phase error Θ changes its amplitude only proportional to Θ^2, while the corresponding complex component with a sine shape is at a zero-crossing and therefore changes linearly with Θ.

If we assume that only one type of nucleus is detected at a time at high field, we can neglect variations of γ_k. Then the multiplicative SNR becomes

$$\frac{\sum_{k=1}^{N} s_k(t)}{n_B(t)} = \frac{i}{B_n \gamma t}\,. \tag{14}$$

This equation states that the sensitivity with respect to B_0 noise is not only independent of the magnetization of the analyte spins, but it is also inversely proportional to γ, *i.e.* low-γ nuclei contribute less to multiplicative noise than high-γ nuclei. In combination with the lower sensitivity of inductive detectors for low-γ nuclei,

this leads to a rapid reduction of the importance of B_0 fluctuations as a source of noise with decreasing γ. Another important aspect of Eq. (14) is its inverse dependence on t, which is correct for time periods during which B_n is approximately constant.

Figure 2 shows the result of a noise analysis in the time domain, where the noise level is shown as a function of the acquisition time t after a single $\pi/2$ pulse. The analysis was done according to Eq. (7) for each point of the ^{1}H as well as the ^{31}P FID of phosphoric acid. Figure 2a shows σ_S as a function of time for both nuclei. Especially in the case of ^{31}P one can see that the additive noise contribution σ_+ cannot be neglected. But because σ_+ can be easily identified (it is the only noise source left when the signal has decayed) and then subtracted using $\sigma_M(t)^2 = \sigma_S(t)^2 - \sigma_+^2$, multiplicative noise can be isolated. Figure 2b shows $\psi_M^{-1}(t) = \sigma_M(t)/|s(t)|$ for ^{1}H and ^{31}P. The two most prominent features in this figure are the increase of the noise relative to the signal, and the higher noise of the nucleus with the larger γ.

If we use t as the independent parameter, we can write the noise afflicted magnetization of each spin component after a detection pulse as

$$M_k^{'+}(t) = M_0 A_k \exp\left(-\frac{t}{T_{2,k}} - i\gamma_k \int_0^t B_0 + B_n(t')\mathrm{d}t'\right) = M_k^+(t) \exp\left(-i\gamma_k \int_0^t B_n(t')\mathrm{d}t'\right), \tag{15}$$

and since $B_n(t)$ is about 10 orders of magnitude smaller than B_0, the signal can be approximated as

$$s'(t) \approx -\sum_{k=1}^{N} i\gamma_k B_0 M_k^{'+}(t) = \sum_{k=1}^{N} s_k(t) \exp\left(-i\gamma_k \int_0^t B_n(t')\mathrm{d}t'\right). \tag{16}$$

Because in the homonuclear case γ_k differ typically only by a few ppm, each component $s_k(t)$ of the FID gets multiplied by the same envelope

$$n^{\mathrm{e}}(t) = \exp\left(-i\gamma \int_0^t B_n(t')\,\mathrm{d}t'\right) \approx 1 - i\gamma \int_0^t B_n(t')\,\mathrm{d}t'. \tag{17}$$

A description of the long-time behavior of phase noise is not straightforward. First of all, B_0 noise is by no means white. It strongly depends on the dominant sources in the environment of the spectrometer as well as the field-frequency lock. This prohibits a generally valid discussion, as there is no fundamental physical process involved that would allow to derive a general expression, and one has to define a model to describe B_0 noise. Let us assume that B_n has a Gaussian probability distribution, a mean value $\langle B_n\rangle = 0$, a variance $\sigma_B^2 = \langle B_n^2\rangle - \langle B_n\rangle^2 = \langle B_n^2\rangle$, and an autocorrelation function

$$\Gamma_B(\tau) = \langle B_n(t)B_n(t+\tau)\rangle = \sigma_B^2 \exp\left(-\frac{|\tau|}{\tau_B}\right) \tag{18}$$

with the correlation time τ_B. The corresponding power spectrum of the B_n noise process,

$$P_B(\omega) = \frac{\sigma_B^2 \tau_B}{\pi\,(1+\omega^2\tau_B^2)}\,, \tag{19}$$

is derived using the Wiener-Khinchin theorem, which states that the autocorrelation function forms a Fourier pair with the power spectral density. This would lead to frequency-independent noise only if $\tau_B \ll \Delta t$, which is generally not correct for B_0 noise. According to Eq. (16), an integration of $B_n(t)$ from the beginning of an FID to time t of the acquisition of a data point,

$$\Theta(t) = \int_0^t B_n(t')\,\mathrm{d}t'\,, \tag{20}$$

is required to characterize the phase error $\Theta(t)$. The variance $\sigma_\Theta(t)^2 = \langle\Theta^2\rangle$ is time dependent,

$$\begin{aligned}\sigma_\Theta(t)^2 &= \left\langle \int_0^t \mathrm{d}t' \int_0^t \mathrm{d}t''\, B_n(t')B_n(t'') \right\rangle = 2\int_0^t \mathrm{d}t'\,(t-t')\,\Gamma_B(t') \\ &= 2\sigma_B^2\tau_B^2\left(\frac{t}{\tau_B} + \exp\left(-\frac{t}{\tau_B}\right) - 1\right)\,. \end{aligned} \tag{21}$$

If $t \ll \tau_B$, this simplifies to $\sigma_\Theta(t)^2 \approx \sigma_B^2 t^2$, and if $t \gg \tau_B$, we get $\sigma_\Theta(t)^2 \approx 2\sigma_B^2\tau_B^2(t/\tau_B - 1) \approx 2\sigma_B^2\tau_B t$. The noise variance evaluates to

$$\sigma_M(t)^2 = \langle [s'(t)-s(t)]\,[s'(t)-s(t)]^*\rangle = |s(t)|^2\,\langle [\exp(-i\gamma\Theta)-1]\,[\exp(i\gamma\Theta)-1]\rangle \tag{22}$$

$$\approx |s(t)|^2\,\langle\gamma^2\Theta^2\rangle = 2\gamma^2\sigma_B^2\tau_B^2\left(\frac{t}{\tau_B} + \exp\left(-\frac{t}{\tau_B}\right) - 1\right)|s(t)|^2\,. \tag{23}$$

For the approximation it was assumed that $|\gamma\Theta| \ll 1$, and the expansion $\exp(\pm i\gamma\Theta) - 1 \approx \pm i\gamma\Theta$ was used. The sensitivity now becomes

$$\psi_B(t) = \frac{|s(t)|}{\sigma_M(t)} = \frac{1}{\sqrt{2\gamma^2\sigma_B^2\tau_B^2\left(\frac{t}{\tau_B} + \exp\left(-\frac{t}{\tau_B}\right) - 1\right)}}\,. \tag{24}$$

The SNR of the two aforementioned extreme cases can be evaluated to be

$$\psi_B(t) \approx \frac{1}{\gamma\sigma_B t} \qquad \text{if } t \ll \tau_B \tag{25}$$

$$\psi_B(t) \approx \frac{1}{\sqrt{2}\gamma\sigma_B\sqrt{\tau_B t}} \qquad \text{if } t \gg \tau_B\,. \tag{26}$$

Eq. (24) shows the same short-time properties as Eq. (14), except that the phase information is lost. The long-time behavior of the multiplicative noise is more like in the case of diffusion [30]. Note that if $T_2 < \tau_B$,

typically only the short-time relation is relevant for practical applications, because for $t > T_2$ the signal decayed to a level where for most samples additive noise is dominant. Equation (24) can now be used to analyze Fig. 2b, where ψ_M^{-1} is plotted. The slope of the two curves is proportional to $1/\gamma$ as predicted. By fitting the data using the ^{1}H data we obtain $\sigma_B = 1.36$ nT and $\tau_B = 0.19$ s. The ^{31}P data, where multiplicative noise is relevant only for about 0.3 s, reveals $\sigma_B = 1.45$ nT and $\tau_B = 0.18$ s. The data was fitted with a non-linear least-square fit using the Levenberg-Marquardt method [31].

Due to the large influence of B_0 fluctuations on multiplicative noise, it can be expected that the field–frequency lock has a considerable impact on this noise source. Figure 3a shows the multiplicative noise with different lock time constants τ_l. $\sigma_B = 2.5$ nT was obtained without lock, and $\sigma_B = 0.43$ nT with $\tau_l = 4.7$ s. With $\tau_l = 1.2$ s the noise at the beginning of the acquisition was about the same as without lock, but at longer t_2 the noise was considerably reduced. However, this curve cannot be reproduced well anymore by Eq. (24). It depends on the dynamics of the lock control system and the solvent used for locking [32]. Experiments with $\tau_l = 12$ s and with $\tau_l = 48$ s gave basically the same result as with $\tau_l = 4.7$ s and are not shown in the figure.

Figure 3b shows the importance of the quality of the lock. Experiments with different lock power settings were recorded. The lock gain was set to its maximum value and the lock power was changed to obtain the lock levels indicated in the figure. Care was taken that at the maximum lock power used in this series the deuterium transition was not saturated. It can be seen that with a more stable lock the multiplicative noise level can be reduced considerably. The results from Fig. 3a were obtained with a lock level corresponding to the highest value in Fig. 3b. The noise levels in the two experiments are therefore comparable. Due to the reduced deuterium concentration in the sample used for Fig. 2, no optimal lock was obtained in that experiment, which explains the increased σ_B compared to the data in Fig. 3.

Coherent Fluctuations of the Static Magnetic Field

Another typical problem is $B_n(t)$ due to a coherent noise source with fundamental frequency ω_c, *e.g.* an AC powered electronic device that is not well shielded. We can make the assumption that

$$B_n(t) = B_\omega \cos\left(\omega_c \left(t + \theta\right)\right) . \tag{27}$$

The coefficient B_ω is constant, and θ denotes a random shift of the noise modulation with respect to the beginning of detection, because usually the experiments are not synchronized with the noise source. If the same integration as in Eq. (20) is performed, we get

$$\Theta_c = \int_0^t B_\omega \cos\left(\omega_c\left(t'+\theta\right)\right)\,\mathrm{d}t' = \frac{2B_\omega}{\omega_c}\cos\left(\omega_c\left(\frac{t}{2}+\theta\right)\right)\sin\left(\frac{\omega_c t}{2}\right). \tag{28}$$

Θ_c is weighted by $1/\omega_c$. This is related to the well-known relation between white noise, which has a frequency-independent power spectrum, and Brownian noise, whose power spectrum shows a $1/f^2$ relation. If white noise is integrated, the resulting noise pattern has a Brownian power spectrum. Although derived here for a non-random modulation, this behavior characterizes also the relation of the spectrum of Θ to the spectrum of $B_n(t)$ for random noise sources. This is of great importance for processes like the free precession of spin magnetization, where phase noise accumulates with time. Low-frequency noise of B_0 has a much bigger influence on the affected process than high-frequency noise. Therefore if slow noise components are present, the influence of fast processes on the observed signal is minor, at least as long as the fast processes are not strongly enhanced, which is sometimes the case for line frequency harmonics.

With coherent noise $\langle s'(t)\rangle$ is not equal to $s(t)$ for all t. The ratio $\langle s'(t)\rangle/s(t)$ can be calculated by noticing that $\omega_c\theta$ is not small compared to unity, and for a large number of co-added identical experiments, the full domain of $\omega_c\theta$ from 0 to 2π is evenly sampled. For the homonuclear case with $\gamma_k \approx \gamma$, we get

$$\frac{\langle s'(t)\rangle}{s(t)} = \frac{\omega_c}{2\pi}\int_{-\pi/\omega_c}^{\pi/\omega_c}\exp\left(-i\,\frac{2\gamma B_\omega}{\omega_c}\sin\left(\frac{\omega_c t}{2}\right)\cos\left(\omega_c\left(\frac{t}{2}+\theta\right)\right)\right)\mathrm{d}\theta\,. \tag{29}$$

By using the expansion $\exp\left(ix\cos\varphi\right) = \sum_{u=-\infty}^{\infty} i^u \mathrm{J}_u(x)\exp\left(iu\varphi\right)$, where J_u is the Bessel function of the first kind, we can rewrite this equation as

$$\frac{\langle s'(t)\rangle}{s(t)} = \frac{\omega_c}{2\pi}\sum_{u=-\infty}^{\infty} i^u \mathrm{J}_u\left(-\frac{2\gamma B_\omega}{\omega_c}\sin\left(\frac{\omega_c t}{2}\right)\right)\exp\left(\frac{iu\omega_c t}{2}\right)\int_{-\pi/\omega_c}^{\pi/\omega_c}\exp\left(iu\omega_c\theta\right). \tag{30}$$

Because u is integer, the integral evaluates to 0 for each u except $u = 0$, and we get

$$\frac{\langle s'(t)\rangle}{s(t)} = \mathrm{J}_0\left(-\frac{2\gamma B_\omega}{\omega_c}\sin\left(\frac{\omega_c t}{2}\right)\right) \approx 1 - \frac{\gamma^2 B_\omega^2}{2\omega_c^2}\left(1-\cos\left(\omega_c t\right)\right). \tag{31}$$

Therefore a second-order component modulated at ω_c remains even with a large number of co-added experiments. This phenomenon is responsible for the well-known sidebands of a liquid sample spinning in

an inhomogeneous field [33, 34]. If the field is very inhomogeneous, the next term in the expansion of the Bessel function might be needed as well, which leads to an additional sideband at $2\omega_c$. If the number of co-added experiments is not sufficiently large to get an ensemble average for each data point of $s(t)$, the simple integration over θ in Eq. (29) cannot be performed. But since the expansion into Bessel functions is still possible, one would have to also consider Bessel functions with $u > 0$ in Eq. (30).

Related to fluctuations of the B_0 field are vibrations of a sample in an inhomogeneous field. In an MAS solid-state NMR experiment, the linewidth can often be shimmed to about 10 Hz, which leaves an average gradient over the sample volume on the order of 1 Hz/mm, and mechanical vibrations of a few microns can lead to an observable level of multiplicative noise.

To calculate the variance caused by a coherent noise source that is not synchronized with the experiment, we can use Eq. (22) and replace Θ with Θ_c from Eq. (28). Analogous to Eqs. (29–31), we obtain

$$\begin{aligned} \sigma_M(t)^2 &= |s(t)|^2 \langle [\exp(-i\gamma\Theta_c) - 1] [\exp(i\gamma\Theta_c) - 1] \rangle \\ &= 2\left[1 - \mathrm{J}_0\left(\frac{2\gamma B_\omega}{\omega_c} \sin\left(\frac{\omega_c t}{2}\right)\right)\right] |s(t)|^2 \approx \frac{\gamma^2 B_\omega^2}{\omega_c^2} \left(1 - \cos\left(\omega_c t\right)\right) |s(t)|^2 \ . \end{aligned} \tag{32}$$

Therefore, transient phase noise caused by a coherent source does not average out even if a large number of experiments with different initial phases are co-added. An example is shown in Fig. 4b, where on top of the increase of $\sigma_S(t_2)$ with rising t_2 a modulation with $\omega_c \approx 16.6$ Hz and $B_\omega \approx 0.5$ nT can be observed. Note that this modulation is indicative of coherent noise that is not synchronized with the experiment. Otherwise it would be only noticeable as a sideband in the spectrum, but not in the transient of the noise variance.

Evolution During rf Irradiation

An on-resonant rf irradiation changes the direction of the magnetization vector $\mathbf{M}_k$ of spin k. The pulse is characterized by its amplitude B_1, by its phase φ_p, by its duration t_p, and by its shape $f_s(t)$. For a rectangular pulse with an excitation bandwidth much broader than the spectrum, the effect on $\mathbf{M}_k$ is described by a flip angle $\beta = -\gamma B_1 t_p$. The problem of noisy rf pulses has been analyzed by different authors [8, 9, 10]. In solid-state NMR experiments, where high rf power is crucial for the success of an experiment and therefore noisier amplifiers with a high gain are used, both phase and amplitude errors are contributing to the total noise [8], while in liquid state experiments, noise due to phase errors is usually dominant [9].

It is possible to determine from time-domain experiments, like the ones in Fig. 2, whether the main cause of multiplicative noise is a phase error accumulated during free precession or fluctuations of the rf pulse. Errors induced by pulses are already present at the beginning of the free evolution period and decay with the same time constant as the signal. Therefore it is advisable to only use the first data point along t_2 to analyze this type of noise, since afterwards phase noise accumulated during t_2 gets admixed.

Within the frame of our simplified classical model, pulse errors can be accounted for by adding a random contribution to A_k. In the case of a pulse with the rf phase in an angle $\phi - \pi/2$ to the reference phase, we get

$$A_k = \frac{M_{0,k}}{M_0} \sin(\beta) \exp(iq_k\phi) \,, \tag{33}$$

where q_k is the order of coherence of the affected transition. The pulses shall be affected by small amplitude errors $\delta\beta$ and phase errors $\delta\phi$. If these errors are time-dependent during the pulse, a similar treatment as described for phase errors due to B_0 fluctuations has to be applied. However, for short pulses we may assume that these errors are constant during one pulse, and uncorrelated for different pulses. For a single pulse, the signal amplitude becomes

$$A_k^{'} = \frac{M_{0,k}}{M_0} \sin(\beta + \delta\beta) \exp\left(iq_k(\phi + \delta\phi)\right) \,, \tag{34}$$

i.e. the error of the pulse amplitude affects only the signal amplitude, and the error of the pulse phase affects only the signal phase. In general we can assume that the amplitude and the phase error are not correlated, so they contribute independently and add in quadrature. In this simple example, we can assume without loss of generality that $\phi = 0$. The error of the flip angle can be caused by a fluctuating B_1 field or a fluctuating t_p. So we can write $\sigma_\beta^2 = \gamma^2(B_1^2\sigma_t^2 + t_p^2\sigma_{B_1}^2)$. The variance of $A_k^{'}$ can then be determined as

$$\sigma_{A_k}^2 = \left|\frac{\partial A_k}{\partial \beta}\right|^2 \sigma_\beta^2 + \left|\frac{\partial A_k}{\partial \phi}\right|^2 \sigma_\phi^2 = \frac{M_{0,k}^2}{M_0^2}\left[\gamma^2\cos^2(\beta)(B_1^2\sigma_t^2 + t_p^2\sigma_{B_1}^2) + \sin^2(\beta)q_k^2\sigma_\phi^2\right] \,. \tag{35}$$

The inherent sensitivity due to this error is

$$\psi_{A_k} = \frac{|s_k|}{\left|\frac{\partial s_k}{\partial A_k}\right| \sigma_{A_k}} = \frac{|A_k|}{\sigma_{A_k}} \approx \frac{1}{\sqrt{\gamma^2\cot^2(\beta)\left(B_1^2\sigma_t^2 + t_p^2\sigma_{B_1}^2\right) + q_k^2\sigma_\psi^2}} \,. \tag{36}$$

This result shows that the relative contribution of the pulse amplitude error gets largest for small flip angles β, because its variance scales with $\cos^2(\beta)$, while the influence of the pulse phase error is most prominent for pulses that are odd integer multiples of $\pi/2$ when $\sin^2(\beta) = 1$. This can be used to optimize pulse flip

angles to minimize multiplicative noise [10]. Furthermore, for certain experiments it is known that basically the same information can be obtained when different coherence transfer pathways are selected. This can be used to reduce the noise by performing the experiment with the lower coherence transfer order [9]. However, note that coherence transfer pathways that are canceled with a phase cycle still contribute to the total multiplicative noise. By dephasing unwanted coherences with gradient filters, also the noise associated with these transitions gets removed. But the B_0 noise is generally higher in the presence of field gradients, which may cause an increase of multiplicative noise on coherences that are not dephased.

In principle, the error of A_k for a single event can be different for each line k of the spectrum. However, especially in the case of non-selective pulses and a spectrum where the lines are not spread over a too wide chemical shift range, the error of A_k for the different lines is correlated or even identical, because the same pulse imperfections act on each spin packet.

In Fig. 2 the contribution of rf pulse fluctuations to the multiplicative noise is approximately $\psi_A \approx 1000$ for ^{1}H. This value represents the maximum achievable multiplicative SNR without signal averaging as limited by the rf pulse reproducibility. The corresponding data is magnified in the inset of Fig. 2b. ψ_A of ^{31}P cannot be determined because additive noise has a higher amplitude than multiplicative noise due to rf pulse fluctuations even at the beginning of the FID.

Interrupted Free Evolution

An rf pulse has also the effect of interrupting the correlation of $M^+(t)$ in a noisy B_0 field. As long as the free evolution periods are longer than τ_B, they are approximatively independent of each other with respect to B_0 noise. If the experiments are executed on a time scale considerably shorter than τ_B, part of the B_0 noise might be refocused at some point, depending on the pulse sequence, but this will not be studied here. The error of different pulses are considered to be uncorrelated, although this assumption can have some limitations for drifts that are induced for example by temperature changes [16].

Because the time scale during which phase errors due to B_0 fluctuations accumulate is usually much longer than the time scale of rf pulses, these two events can be treated independently. Furthermore a pulse that converts one component of coherent magnetization into polarization also transfers a phase into an amplitude error. Therefore the multiplicative noise due to different pulses and interrupted free evolution

periods adds up according to Eq. (1). On the other hand, all the spins in a molecule experience the same fluctuations from the noisy quantities that influence the signal, so this noise adds up linearly. If more than one pulse is applied, the simple dependence of amplitude errors on $\cos(\beta)$ and phase errors on $\sin(\beta)$ is not valid anymore. For a quantitative description it is then necessary to analyze each pulse sequence separately [10]. For a qualitative upper limit estimate, we can replace $\cos(\beta)$ and $\sin(\beta)$ with 1. Relaxation terms are not considered, because multiplicative noise relaxes with the same rate as the signal. Depending on the applied pulse sequence, also multiple quantum coherences can occur at some point during an experiment. This scales the precession frequency of the magnetization and therefore also the phase errors due to B_0 fluctuations with the order q_m of the specific coherence. If we consider only a single coherence pathway from a single line, we get

$$\begin{aligned} \psi_M(t)^2 &= \frac{|s(t)|^2}{\sigma_M(t)^2} = \frac{|s(t)|^2}{\sum_{p=1}^{P} \left(\frac{\partial s}{\partial A}\right)^2 \sigma_A^2 + \left(\frac{\partial s}{\partial B_0}\right)^2 \sigma_B^2} \\ &= \left[\sum_{m=1}^{P} \gamma^2 (B_{1,m}^2 \sigma_{t_{p,m}}^2 + t_{p,m}^2 \sigma_{B_{1,m}}^2) + q_m^2 \sigma_{\phi_m}^2 + 2 q_m^2 \gamma^2 \sigma_B^2 \tau_B^2 \left(\frac{t_m}{\tau_B} + \exp\left(-\frac{t_m}{\tau_B}\right) - 1\right)\right]^{-1} . \end{aligned} \tag{37}$$

P is the total number of pulses, and t_m is the evolution time after pulse m. t_2 is the transient evolution during detection[1], thus $|q_2| = 1$.

To apply the simplified classical scheme to discuss multi-pulse experiments, the noise from each free evolution period and from each pulse must be determined for each signal component k, *i.e.* each coherence pathway for each spin. Exact values of $A_{k,m}$ have to be determined with a quantum mechanical treatment, but this is out of the scope of this discussion. To fully account for multiplicative noise, a sum has to be taken over all the coherences that finally evolve into observable magnetization, even if they are phase-cycled out. As can be anticipated from Eq. (37), general expressions become very complicated, but with some realistic assumptions useful conclusions regarding the sensitivity are still possible.

[1] For consistency with other equations, t_1 is the time that is increased in the indirect dimension, and t_2 the transient evolution time; all the other events in Eq. (37) shall be ordered chronologically.

Recycle Delay and Noisy Initial Conditions

For the interpretation of multi-dimensional NMR data, it is usually assumed that when the first pulse is applied at the beginning of each trace, the magnetization $\mathbf{M}$ has always the same value. If the recycle delay between two subsequent traces is very long such that the spin magnetization can reach its Boltzmann equilibrium value $\mathbf{M}_0$, this assumption is justified very well because $\mathbf{M}_0$ is basically noiseless at the level of accuracy available in an NMR experiment, provided that the temperature of the sample is stable. But one usually cannot afford to wait "infinitely" long between subsequent repetitions. A certain fraction of encoded magnetization survives, which appears in the spectrum as if the same pulse sequence were applied twice, giving rise to additional coherences [35] that are not suppressed with the usual phase cycles. The safest way to avoid such coherences is to wait for $t_r \geq 5T_1$, where t_r is the recycle delay between the last pulse of a certain trace and the first pulse of the next trace. Then $M_z(t_0)/M_0 > 0.99$, where t_0 denotes the time immediately before the first pulse of each trace. These additional coherences can also be phase-cycled out [36], but if M_z is affected by multiplicative noise, some of this noise is handed down to the next trace of the experiment. This is one mechanism for a correlation of multiplicative noise between different traces. If we assume that no additional multiplicative noise is added to longitudinal magnetization during a free evolution, and that this noise contribution relaxes with the same T_1 as the magnetization of the spins it is imposed on, the inherited noise at the beginning of a new trace is

$$\sigma_z(t_0) = \sigma_z(t_e)\, \exp\left(-\frac{t_r}{T_1}\right) , \tag{38}$$

where t_e describes the moment right after the last pulse of a certain trace of the experiment, and $\sigma_z(t_e)$ is the standard deviation of the noise of $M_z(t_e)$. In a series of identical experiments, the longitudinal magnetization $M_z^{(p+1)}(t_0)$ at the beginning of experiment number $(p+1)$ can be calculated recursively as

$$M_z^{(p+1)}(t_0) = M_0 + \left(M_z^{(p)}(t_0)\alpha(t_1) - M_0\right) \exp\left(-\frac{t_r}{T_1}\right) , \tag{39}$$

where $\alpha(t_1) = M_z^{(p)}(t_e)/M_z^{(p)}(t_0)$. After an infinite number of experiments with identical t_1, we get

$$\frac{M_z^{(\infty)}(t_0)}{M_0} = \frac{1 - \exp\left(-\frac{t_r}{T_1}\right)}{1 - \alpha(t_1)\exp\left(-\frac{t_r}{T_1}\right)} . \tag{40}$$

If we consider as a didactic example a COSY experiment [2] with two ideal non-selective $\pi/2$ pulses separated by t_1 (Fig. 5a), the transverse magnetization of an isolated spin at time t_1 after the first pulse of trace p

is $M^+(t_1) = M_z^{(p)}(t_0)\exp(-t_1/T_2 + i\omega t_1)$. By the second pulse, one component of M^+ is stored as z magnetization, say $M_z^{(p)}(t_e) = M_z^{(p)}(t_0)\exp(-t_1/T_2)\cos(\omega t_1)$, thus $\alpha(t_1) = \exp(-t_1/T_2)\cos(\omega t_1)$. We then can determine $M_z^{(\infty)}/M_0$ for different values of t_r/T_1 (Fig. 5b). In Fig. 5c, $M_z^{(p)}(t_0)/M_0$ is shown for an increasing number of p. Let us assume that the main source of multiplicative noise is due to phase errors accumulated during t_1 and stored as longitudinal magnetization by the second pulse. According to Eq. (14), this noise is out-of-phase with the precessing magnetization, therefore we get

$$\sigma_z^{(1)}(t_e) = \gamma\sigma_B t_1 \exp\left(-\frac{t_1}{T_2}\right)|\sin(\omega t_1)|\, M_0 \tag{41}$$

after the second $\pi/2$ pulse of the first trace. If multiple traces of the same experiment are recorded, the inherited noise from each of them adds in quadrature, and one recursively gets

$$\sigma_z^{(p+1)}(t_0) = \sqrt{\left[\gamma\sigma_B t_1 \exp\left(-\frac{t_1}{T_2} - \frac{t_r}{T_1}\right)\sin(\omega t_1) M_z^{(p)}(t_0)\right]^2 + \left[\sigma_z^{(p)}(t_0)\exp\left(-\frac{t_1}{T_2} - \frac{t_r}{T_1}\right)\right]^2} \tag{42}$$

at the beginning of a new trace. This step can be repeated over several generations, and assuming that all the experiments were done with the same t_1, the relation

$$\sigma_z^{(n+1)}(t_0) = \gamma\sigma_B t_1 \exp\left(-\frac{t_1}{T_2} - \frac{t_r}{T_1}\right)|\sin(\omega t_1)| \sqrt{\sum_{p=0}^{n}\left[M_z^{(p)}(t_0)\exp\left(-\frac{t_1}{T_2} - \frac{t_r}{T_1}\right)^{n-p}\right]^2} \tag{43}$$

is obtained. For an infinite number of experiments, one gets for the inherited sensitivity

$$\psi_z^{(\infty)}(t_0) = \frac{M_z^{(\infty)}(t_0)}{\sigma_z^{(\infty)}(t_0)} \approx \frac{\sqrt{\exp\left(2\left(\frac{t_1}{T_2} + \frac{t_r}{T_1}\right)\right) - 1}}{\gamma\sigma_B t_1 \left|\sin(\omega t_1)\right|}\,. \tag{44}$$

The approximation assumes $M_z^{(p)}(t_0) \approx M_z^{(\infty)}(t_0)$, which allows to use the relation $\sum_{p=0}^{\infty}\exp(-x)^p = (1 - \exp(-x))^{-1}$ for $x > 0$. If coherence evolves at order q during t_1, $\psi_z^{(\infty)}(t_0)$ scales with q^{-1}.

In [11] a 2D experiment was presented with hyperpolarized xenon, where during each repetition only a small fraction of the available magnetization was used. To minimize the loss of magnetization due to T_1 relaxation of the xenon, a short t_r was desirable. It was observed experimentally that inheritance of noise can indeed have a considerable influence on the performance of such an experiment. However, since fluctuations of B_0 are slow, increasing t_r increases the influence of very slow B_0 fluctuations, even with the field–frequency lock turned on. Figure 4 shows the influence of t_r for the case where $t_r \geq 5T_1$. In Fig. 4a a tendency can be observed that with a longer recycle delay the multiplicative noise level is getting higher. Since all the curves

begin at $\sigma_S(t)/s(t) \approx 0$, inheritance of noise between experiments is low even for the shortest recycle delays. The experiments were recorded one right after the other, starting with the shortest recycle delay. But this result indicates only a trend. Another experiment with a recycle delay of $t_r = 30$ s, but otherwise identical settings, was recorded during the night when activity in the lab is low and the temperature in the room is known to be more stable. It showed a noise level that was almost as low as the one with $t_r = 1.5$ s. To verify this trend, additional experiments were done on a different spectrometer in a different room. Figure 4b was obtained with the 700 MHz spectrometer. The same tendency was observed, but this time less pronounced.

IMPACT OF MULTIPLICATIVE NOISE ON THE SPECTRUM

If multiplicative noise is small compared to the signal so that we can write a noisy time domain transient as

$$s'(t) = s(t)\ (1 + \xi_M(t))\ , \tag{45}$$

where $\xi_M(t)$ is a complex random variable with Gaussian probability distribution and zero mean, then the noise in the frequency domain is

$$S'(\omega) - S(\omega) = S(\omega) \otimes \mathcal{N}(\omega)\,, \tag{46}$$

where $S'(\omega)$, $S(\omega)$, and $\mathcal{N}(\omega)$ are the Fourier transforms of the noisy signal $s'(t)$, the noiseless signal $s(t)$, and $\xi_M(t)$, respectively. This convolution, denoted by $\otimes$, is the reason why multiplicative noise that appears in the spectrum is not due to noise sources that have the same frequency as the Larmor frequency of the spins, but it is low frequency noise within the bandwidth of the receiver.

White additive noise gives the same offset-independent SNR in the direct and the indirect dimension of a 2D spectrum, because its correlation time is much shorter than the time scale of NMR experiments. For multiplicative noise, the direct and the indirect dimensions of a multidimensional spectrum show different properties. The different situations how noise acts on the spectrum are shown in Fig. 6. Additive noise adds to the signal in both the time and the frequency domain (Fig. 6b), while according to Eq. (46), noise that is multiplicative in the time domain corresponds to a convolution of the FT of the noise with the noiseless spectrum in the frequency domain (Figs. 6c-f). In the direct as well as in the indirect dimension, noise added during the time period which is increased (t_1 in the indirect and t_2 in the direct dimension) has to be distinguished from noise added during all the other parts of an experiment.

Most noise-inducing processes lead dominantly either to phase noise or to amplitude noise. In the case of phase noise like in Eq. (17), $\xi_M(t)$ is imaginary, and

$$\mathcal{N}(-\omega) = -\mathcal{N}^*(\omega)\,. \tag{47}$$

In the case of amplitude noise, $\xi_M(t)$ is real, thus

$$\mathcal{N}(-\omega) = \mathcal{N}^*(\omega)\,. \tag{48}$$

These relations can often be used to identify the source of multiplicative noise. For example, the cause of rf pulse fluctuations can be investigated by taking the first data point of an FID from a set of identical experiments and perform an FT along the "signal averaging" dimension. If this first point is at the origin of a cosine modulation so that its imaginary component is zero, pure phase noise of the pulse leads to a noise spectrum that behaves according to Eq. (47), while pure amplitude noise causes the noise spectrum to follow Eq. (48). This is demonstrated with a one-pulse FID experiment that was repeated 100 times at a proton frequency of 700 MHz, using a sample of 1% H_2O in D_2O, doped with 0.1 g/l $GdCl_3$ (4 Hz H_2O/D_2O sample, dist. by Varian, Palo Alto, CA). Figure 7 shows that the fluctuations of the rf pulses are not completely white in this case, but that there is an increased low frequency component. All the high frequency noise complies with the relation for phase noise. Most of the low frequency noise is phase noise as well, but there is another contribution of different origin, like a drift of the circuit tuning or of the rf amplifier gain. Note that the bandwidth in Fig. 7 is given by the repetition rate of the experiment, and the resolution by the inverse of the total time to record all the identical data sets.

Direct Dimension

Multiplicative noise sources that affect the spins prior to detection simply scale each line in each t_2 transient by a certain factor and can be described by the variance $\sigma^2_{A_k}$ of A_k at the beginning of an acquisition. σ_{A_k} includes all the noise that accumulated during rf pulses and free evolutions up to that point. Assuming that each spin is affected equally by multiplicative noise, all the lines in the spectrum get scaled by the same factor, which neither adds frequency-dependent random noise nor influences the lineshape in the direct dimension. But it does affect the reproducibility of an experiment, and its influence becomes visible when certain coherences are to be suppressed in a phase cycle. This situation is shown in Fig. 6c. Every time

one component of the precessing magnetization is transfered to polarization with an rf pulse, a phase error is converted into an amplitude error. Therefore $\xi_M(t)$ is typically dominantly real. A phase error of the detection pulse, however, leads to a phase error in the signal.

For a certain t_1, $\tilde{\psi}_{A_k}(0)$ in the frequency domain is identical to ψ_{A_k} in the time domain, which is equal to $\psi_M(t)$ in Eq. (37) minus the contribution accumulated during t_2. The sensitivity as a function of the frequency offset for a single line is

$$\tilde{\psi}_A(\Delta\omega_n) = \sqrt{1+\Delta\omega_n^2\tau_2^2}\left[\sum_{l=1}^{L}\tilde{\psi}_{A_l}^{-2}(0)\right]^{-1/2} . \tag{49}$$

τ_2 is the signal lifetime along t_2, $\Delta\omega_n = 0$ corresponds to the center of the line after a discrete Fourier transform, and l counts through all the statistically independent events and all the coherence pathways that contribute to this line. For each l, a different ψ_{A_l} can be determined. Equation (49) can be used to calculate the standard deviation in the frequency domain as

$$\tilde{\sigma}_A(\Delta\omega_n) = \frac{|S(0)|}{\tilde{\psi}_A(\Delta\omega_n)} = \frac{s_0\left(1-\exp\left(-\dfrac{T}{\tau_2}\right)\right)}{T\sqrt{\tau_2^{-2}+\Delta\omega_n^2}\,\tilde{\psi}_A(0)} , \tag{50}$$

where T is the length of each transient data trace, and $s_0 = s(0)$ in the time domain. The noise has the same $\Delta\omega_n$ dependence as the line itself, therefore no sensitivity is gained or lost for this kind of noise with a matched filter or any other apodization.

Multiplicative noise that adds during detection behaves differently. It changes its value during data acquisition, and a single transient signal can be summarized as

$$s'(t) \approx \sum_{k=1}^{N} s_k(t)\,\exp\left(-i\gamma\Theta(t)\right) \approx \sum_{k=1}^{N} s_k(t)\,\left(1-i\gamma\Theta(t)\right) . \tag{51}$$

In the time domain, this states that each spin accumulates the same phase error during a particular evolution period. If this were the only noise source in the frequency domain, $\mathcal{N}(\omega)$ would behave according to Eq. (47). The result is shown in Fig. 6d. In 1D experiments where the spectrum is phased and only the absorptive part is retained, phase noise gets converted into an antisymmetric distortion of each line.

For a more quantitative discussion of multiplicative noise that adds during t_2, the situation with and without relaxation will be considered independently. Without relaxation, the time-domain signal is $s(t) = s_0$ if we assume for now that the carrier frequency is equal to the resonant frequency of the transition. The

on-resonant line intensity in the frequency domain is

$$S(0) = \frac{1}{T}\int_0^T s(t)\,\mathrm{d}t = s_0\,. \tag{52}$$

In the direct dimension, $T \ll \tau_B$ will be assumed. Then the main influence of multiplicative noise can be approximated by the short-time approximation of Eq. (23), *i.e.* $\sigma_M(t) \approx |s(t)|\,\gamma\sigma_B t$. The SNR can be calculated by dividing the on-resonant signal by the Fourier series of the noise. This is permitted because the time-domain noise in the direct dimension is a continuous function whose amplitude B_n changes from experiment to experiment, but with a stable power spectrum. If we neglect relaxation, thus $|s(t)| = s_0$, we get

$$\tilde{\sigma}_T(\Delta\omega_n) = \left|\frac{1}{T}\int_0^T |s(t)|\,\gamma\sigma_B t \exp\left(-i\,\frac{2\pi n t}{T}\right)\,\mathrm{d}t\right| = \begin{cases} \dfrac{\gamma\sigma_B T s_0}{2} & n = 0 \\ \dfrac{\gamma\sigma_B s_0}{\Delta\omega_n} & |n| > 0\,, \end{cases} \tag{53}$$

with $\Delta\omega_n = 2\pi n/T$. With $S(0)$ given by Eq. (52), the sensitivity as a function of the off-resonance frequency is

$$\tilde{\psi}_T(\Delta\omega_n) = \begin{cases} \dfrac{2}{\gamma\sigma_B T} & n = 0 \\ \dfrac{\Delta\omega_n}{\gamma\sigma_B} & |n| > 0 \end{cases} \tag{54}$$

The noise is inversely proportional to $\Delta\omega_n$. At spectral regions that are not in the direct vicinity of any lines, no contribution from multiplicative noise remains, and the noise is purely given by additive noise. Thus in a 1D spectrum with transient detection usually only additive noise is noticed as the limiting contribution. This also shows the importance to suppress low frequency fluctuations of B_0.

With relaxation included, the signal shall be $s(t) = s_0 \exp(-t/\tau_2)$, and the on-resonant line intensity is

$$S_0 = S(0) = s_0\frac{\tau_2}{T}\left(1 - \exp\left(-\frac{T}{\tau_2}\right)\right)\,. \tag{55}$$

The noise becomes

$$\begin{aligned} \tilde{\sigma}_T(\Delta\omega_n) &= \left|\frac{1}{T}\int_0^T s_0 \exp\left(-\frac{t}{\tau_2}\right)\gamma\sigma_B t \exp\left(-\frac{i2\pi n t}{T}\right)\,\mathrm{d}t\right| \\ &= \frac{s_0\gamma\sigma_B\tau_2^2}{T\,(1+\omega_n^2\tau_2^2)}\sqrt{\left(1 - \exp\left(-\frac{T}{\tau_2}\right)\left(1+\frac{T}{\tau_2}\right)\right)^2 + \omega_n^2 T^2 \exp\left(-\frac{2T}{\tau_2}\right)}\,. \end{aligned} \tag{56}$$

If we assume that $T \gg \tau_2$, this simplifies to

$$\tilde{\sigma}_T(\Delta\omega) = \frac{s_0\gamma\sigma_B\sqrt{T^{-2} + \Delta\omega_n^2 \exp\left(-\dfrac{2T}{\tau_2}\right)}}{\tau_2^{-2} + \Delta\omega_n^2} \approx \frac{s_0\gamma\sigma_B\tau_2^2}{T\left(1 + \Delta\omega_n^2\tau_2^2\right)}\,. \tag{57}$$

The approximation is valid in the vicinity of $\Delta\omega_n = 0$. On-resonant, the multiplicative noise limited sensitivity is $\tilde{\psi}_T(0) = [\gamma\sigma_B\tau_2]^{-1}$ and thus proportional to the inverse of τ_2, which is in contrast to the additive noise limited sensitivity. The sensitivity close to resonance is

$$\tilde{\psi}_T(\Delta\omega_n) = \frac{1 + \Delta\omega_n^2\tau_2^2}{\gamma\sigma_B\tau_2}\,, \tag{58}$$

again assuming that $T \gg \tau_2$. This kind of noise has a different dependence on ω_n than the signal. On-resonant, the sensitivity can be optimized by reducing τ_2, while off-resonant a longer τ_2 is advantageous. Note that because the noise is proportional to the signal, it does not matter sensitivity-wise if τ_2 is the decoherence time T_2 of the sample, or if it is the time constant of an apodization function. It is the combined effect of relaxation and apodization that matters. If Eq. (57) is combined with the multiplicative noise that accumulated prior to detection, given by Eq. (50), we get

$$\tilde{\sigma}_M(\Delta\omega_n) = \sqrt{\sigma_A^2(\Delta\omega_n) + \sigma_T^2(\Delta\omega_n)} = \frac{s_0\tau_2}{T\sqrt{1 + \Delta\omega_n^2\tau_2^2}}\sqrt{\frac{1}{\tilde{\psi}_A(0)^2} + \frac{\gamma^2\sigma_B^2\tau_2^2}{1 + \Delta\omega_n^2\tau_2^2}}\,. \tag{59}$$

The above equations were derived assuming no signal averaging. If N_S identical experiments are co-added or a phase cycle with N_S steps is applied, the on-resonant sensitivity becomes

$$\tilde{\psi}_M(0) = \sqrt{\frac{N_S}{\gamma^2\sigma_B^2\tau_2^2 + \psi_A(0)^{-2}}}\,. \tag{60}$$

This equation defines the sensitivity of one data point along t_1, which is needed later to discuss the sensitivity along the indirect dimension of a 2D spectrum.

The sensitivity of a ^{1}H spectrum at 300 MHz in the direct dimension is shown in Fig. 8. The sample was a solution of 1 M NaCl dissolved in H_2O:D_2O (1:1) that also contained a small amount of isopropyl alcohol (EMD Chemicals Inc., Gibbstown NJ). On-resonant the noise is highest, and phase noise as described by Eq. (57) is dominant. Noise due to pulse imperfections, given by Eq. (50), becomes more important off-resonant. Additive noise finally becomes dominant far off-resonant. An additional feature of this noise spectrum are the lines from coherent noise sources at $|\Delta\omega|/2\pi = 60$ Hz and multiples thereof. Additionally

there is a distinct sideband at $|\Delta\omega|/2\pi = 75$ Hz of unknown origin. Furthermore, emphasized by an arrow in the figure, the multiplicative noise from the five strongest lines of the isopropyl alcohol septet is visible. These lines are much more prominent in the noise spectrum than in the real spectrum. The deviation of the experimental from the calculated noise in Fig. 8 is primarily because of a non-exponential decay of the signal due to imperfect shimming.

The same experimental data as for Fig. 7 was used to analyze the noise in the direct dimension. The data was Fourier transformed along the direct dimension only (Fig. 9a). The absolute value of a data point in both wings of a line with equal distance to its center is shown in Fig. 9b. The signal is stable around a mean value, and the noise is antisymmetric with respect to the center of the line, which complies with Eq. (47) and is as expected for phase fluctuations. That the noise is correlated is shown in Fig. 9c, where the absolute value of two adjacent points in the spectrum is shown. Figure 9d shows the effect of reducing τ_2 by changing the apodization function. As predicted the on-resonant sensitivity gets improved by shorter τ_2, while the off-resonant sensitivity decreases. Because the initial relaxation pattern is not perfectly exponential, the unfiltered shape of the sensitivity does not match Eq. (56). The shorter τ_2 was made by apodization, the better the experimental result agreed with the theoretical.

Indirect Dimension

Along the indirect dimension, the B_0 noise of subsequent traces is ideally uncorrelated. Therefore multiplicative noise along the indirect dimension is white and spreads over the whole bandwidth of the F_1 dimension. Any correlation of multiplicative noise would be either due to a short recycle delay and inheritance of noise, or due to noise processes with a correlation time slower than the repetition time of the experiment. But still all the different spin packets experience the same B_0 and are affected in the same way by rf pulse fluctuations, at least as long as the spectrum is excited evenly with non-selective pulses. Thus also along the indirect dimension each line gets convoluted with the same noise pattern. Because each of these noise spectra is shifted by the offset of the line with respect to each other, the total multiplicative noise scales in quadrature with the intensity of each line.

For a quantitative estimate, let us look at the sensitivity of one trace along the indirect dimension that is on-resonant with a line in the direct dimension. Like in the direct dimension, noise that accumulates during

t_1 has to be treated separately from noise that is accumulated prior or after t_1. The signal shall have the same form as described by Eqs. (2) and (3), except that γ_k must be substituted by $q_k\gamma_k$. Because the noise is uncorrelated along t_1, it gets evenly redistributed by the FT, and the sensitivity is identical for each value of the offset frequency $\Delta\omega_1$. The average noise variance at each point along F_1 in the absence of relaxation along t_1 can be calculated from Eq. (60) as

$$\tilde{\sigma}_{A_0}^{(1)} = \sqrt{\frac{\tilde{s}_0^2}{N_S K_1^2}\sum_{k=1}^{K_1}\left[\gamma^2\sigma_B^2\tau_2^2 + \tilde{\psi}_{A'}(0)^{-2}\right]} = \frac{\tilde{s}_0}{\sqrt{N_S K_1}}\sqrt{\gamma^2\sigma_B^2\tau_2^2 + \tilde{\psi}_{A'}(0)^{-2}} \tag{61}$$

for the noise accumulating prior and after t_1, and

$$\tilde{\sigma}_{T_0}^{(1)} = \sqrt{\frac{\tilde{s}_0^2}{N_S K_1^2}\sum_{k=1}^{K_1} q^2\gamma^2\sigma_B^2\Delta t_1^2 k^2} \approx \tilde{s}_0 q\gamma\sigma_B\Delta t_1\sqrt{\frac{K_1}{3N_S}} \tag{62}$$

for the noise accumulating during t_1. K_1 is the number of data points along t_1, Δt_1 is the distance between them, and $\tilde{s}_0 = s_0\tau_2/T$. $\tilde{\psi}_{A'}(0)$ is given by Eq. 49, except that the noise accumulated during the t_1 evolution is excluded. It was assumed that $t_1^{\max} = K_1\Delta t_1 \ll \tau_B$. We can calculate the sensitivity in the absence of relaxation as

$$\tilde{\psi}_{M_0}^{(1)} \approx \sqrt{\frac{N_S K_1}{\gamma^2\sigma_B^2\tau_2^2 + \tilde{\psi}_{A'}(0)^{-2} + q^2\gamma^2\sigma_B^2(t_1^{\max})^2/3}}\,. \tag{63}$$

If we consider relaxation along t_1, the noise accumulating prior and after t_1 is

$$\begin{aligned}\tilde{\sigma}_A^{(1)} &= \tilde{\sigma}_{A_0}^{(1)}\sqrt{\sum_{k=-\infty}^{\infty}|S_{\mathrm{e}}(\omega_k)|^2} = \tilde{\sigma}_{A_0}^{(1)}\left(1-\exp\left(-\frac{t_1^{\max}}{\tau_1}\right)\right)\sqrt{\sum_{k=-\infty}^{\infty}\left[\left(\frac{t_1^{\max}}{\tau_1}\right)^2 + (2\pi k)^2\right]^{-1}} \\ &= \tilde{\sigma}_{A_0}^{(1)}\left(1-\exp\left(-\frac{t_1^{\max}}{\tau_1}\right)\right)\sqrt{\frac{\tau_1\coth\left(\frac{t_1^{\max}}{2\tau_1}\right)}{2t_1^{\max}}}\,,\end{aligned} \tag{64}$$

assuming that the bandwidth of the spectrum is considerably broader than the linewidth. τ_1 is the signal lifetime along t_1, and $S_{\mathrm{e}}(\omega_k) = S(\omega_k)/\tilde{s}_0$ is the normalized lineshape function along F_1. The normalized on-resonant signal along F_1 is $S_{\mathrm{e}}(0) = (1-\exp(-t_1^{\max}/\tau_1))(\tau_1/t_1^{\max})$.

Figure 6e shows an example of multiplicative noise along the indirect dimension if noise is dominant that does not accumulate during t_1. The sensitivity in this case is

$$\tilde{\psi}_A^{(1)} = \frac{\tilde{s}_0\frac{\tau_1}{t_1^{\max}}\left(1-\exp\left(-\frac{t_1^{\max}}{\tau_1}\right)\right)}{\tilde{\sigma}_A^{(1)}} \approx \frac{\sqrt{N_S K_1}}{\sqrt{\gamma^2\sigma_B^2\tau_2^2 + \tilde{\psi}_{A'}(0)^{-2}}\left(1+\frac{1}{24}\left(\frac{t_1^{\max}}{\tau_1}\right)^2\right)}\,. \tag{65}$$

The approximation is valid for $t_1^{\max} < 2\tau_1$, which is reasonable in the indirect dimension where sensitivity and total experiment time considerations usually do not allow to record data points until the signal has fully decayed. According to Eq. (65), changing τ_1 with an apodization function has no big effect on the sensitivity due to non-transient multiplicative noise as long as $\tau_1 > t_1^{\max}$. However, if $\tau_1 < t_1^{\max}/2$ the sensitivity drops considerably.

Noise that adds during t_1 accounts for

$$\begin{aligned}\tilde{\sigma}_T^{(1)} &= \sqrt{\frac{\tilde{s}_0^2}{N_S K_1^2}\sum_{k=1}^{K_1} q^2\gamma^2\sigma_B^2\Delta t_1^2 k^2 \exp\left(-\frac{2\Delta t_1 k}{\tau_1}\right)} \\ &\approx \frac{\tilde{s}_0 q\gamma\sigma_B\tau_1}{2\sqrt{N_S K_1}}\sqrt{\frac{\tau_1}{t_1^{\max}} - \exp\left(-\frac{2t_1^{\max}}{\tau_1}\right)\left(\frac{\tau_1}{t_1^{\max}} + \frac{1}{2}\left(1 + \frac{t_1^{\max}}{\tau_1}\right)\right)}. \end{aligned} \tag{66}$$

In this case, the shorter τ_1 in an apodization function, the better the sensitivity becomes. Figure 6f shows the situation with noise adding during the t_1 evolution as the main multiplicative noise source.

If we have N lines along F_1 which do not overlap, the noise scales with

$$\tilde{\sigma}_M^{(1)} = \sqrt{\sum_{n=1}^{N}\left[\tilde{\sigma}_{A,n}^{(1)}\right]^2 + \left[\tilde{\sigma}_{T,n}^{(1)}\right]^2}. \tag{67}$$

For the case of identical τ_1 of all lines along t_1, we get an SNR for line k that is proportional to

$$\tilde{\psi}_{M,k}^{(1)} \propto \frac{\tilde{s}_{0,k}}{\sqrt{\sum_{n=1}^{N}\tilde{s}_{0,n}^2}} \tag{68}$$

This result shows that noise along F_1 due to a large diagonal peak can suppress weak cross-peaks even if their amplitude is above the level of the additive noise, which is especially severe at the spectral position of a solvent peak.

UNSTABLE RF CIRCUIT

Mechanical vibrations of the rf circuit or temperature changes can induce a variation of the phase of the signal with respect to the reference phase [15, 16]. These phase changes are caused by a fluctuation of capacitances, inductances, and possibly resistances that define the circuit. They can be analyzed using the transfer function $H(\omega)$ of the resonant circuit. Alternatively, this problem could also be discussed with the

impedance as the relevant quantity. An analytical description is possible, but it is usually demanding for any circuit of practical relevance. The effect of vibrations largely depends on which part of the electronic circuit is mainly affected, and the existence of stray capacitances and inductances or problems with the grounding can complicate the situation further.

In a very simplified model we can consider a serial resonant circuit consisting of a coil with inductance L, a capacitance C, and a resistance R (Fig. 10a). The resonance condition is $\omega_0 = 1/\sqrt{LC}$, and the quality factor is $Q = \omega_0 L/R = \sqrt{L/C}/R$, where usually $Q \gg 1$. The vibrations mainly affect L and C, giving rise to the variances σ_L^2 and σ_C^2, respectively. The noise will be described by the variance σ_H^2 of $|H(\omega)|$ and σ_α^2 of the phase $\alpha(\omega)$ of $H(\omega)$. An additional simplification is to consider only stationary oscillations if we assume the ringing to be very short compared to the length of the overall excitation or signal. For detection, this assumption is fulfilled very well, because the first point cannot be recorded anyway until the ringing caused by the rf irradiation has decayed, and Δt is typically considerably longer than the time constant $\tau_d = 2Q/\omega_0$ of the resonant circuit. For the rf irradiation itself, the rise and fall time of the pulse can only be neglected if the pulse is several times longer than τ_d.

If we consider the case of detection where the excitation of the circuit is due to the precession of M^+ inside the coil and the signal is detected as the voltage across the capacitor, and we represent the stationary part of a forced oscillation in a complex notation with $w_o(t) = W_o(\omega)\exp(i\omega t)$, the amplitude of the stationary oscillation W_o relative to the amplitude of the excitation W_e is

$$H(\omega) = \frac{W_o}{W_e} = \frac{1}{1 - \left(\frac{\omega}{\omega_0}\right)^2 + i\frac{\omega}{Q\omega_0}} \approx \frac{1}{2\frac{\Delta\omega}{\omega} + \frac{i}{Q}}\,, \tag{69}$$

where ω is the frequency of the precessing magnetization and $\Delta\omega = \omega_0 - \omega$. The resonance frequency ω_0 of the circuit is characterized by a vanishing imaginary part of the impedance. To obtain physically interpretable correlations, it can be useful to split the analysis into two steps, first a calculation of how $H(\omega)$ is affected by a fluctuation of the resonance frequency ω_0 of the circuit, and then how ω_0 is affected by a fluctuation of L and C. Furthermore, amplitude and phase errors of $H(\omega)$ are of importance independently of each other [16], thus it is useful to discuss them separately. Eq. (69) becomes particularly simple if $\omega = \omega_0$.

If we assume ω to be noiseless and ω_0 to be noisy, we get

$$\frac{\partial|H|}{\partial\omega_0} = -\frac{\omega^2}{\omega_0^3}\frac{2\left(1-\left(\frac{\omega}{\omega_0}\right)^2\right)-\frac{1}{Q^2}}{\left[\left(1-\left(\frac{\omega}{\omega_0}\right)^2\right)^2+\frac{\omega^2}{Q^2\omega_0^2}\right]^{3/2}} \approx -\frac{1}{\omega}\frac{4\frac{\Delta\omega}{\omega}-\frac{1}{Q^2}}{\left[\left(2\frac{\Delta\omega}{\omega}\right)^2+\frac{1}{Q^2}\right]^{3/2}}, \tag{70}$$

$$\frac{\partial\alpha}{\partial\omega_0} = \frac{\omega(\omega_0^2-\omega^2)-2\omega\omega_0^2}{Q\left(\omega_0^2-\omega^2\right)^2+\frac{\omega^2\omega_0^2}{Q}} \approx -\frac{1}{\omega}\frac{1}{2Q\left(\frac{\Delta\omega}{\omega}\right)^2+\frac{1}{2Q}}. \tag{71}$$

For the approximation, we used $\omega_0^2-\omega^2 \approx 2\Delta\omega\omega$. Note the very high sensitivity on $\Delta\omega$. So even if we assume that $\langle\omega_0\rangle = \omega$, we still need to consider $\Delta\omega$ in these equations, otherwise their validity range is too limited. Furthermore, $\langle|H(\omega)|\rangle$ depends on $\Delta\omega$, and therefore in a noisy environment on σ_ω^2, the variance of ω_0. For this example, let us assume that L is the dominant noisy quantity in the resonant circuit. From $\omega_0 = 1/\sqrt{LC}$ we get

$$\frac{\partial\omega_0}{\partial L} = -\frac{1}{2\sqrt{L^3C}} = -\frac{\omega_0}{2L}, \tag{72}$$

and substituting $\partial\omega_0$ with $\Delta\omega$ and ∂L with ΔL, we get approximately

$$\frac{\Delta\omega}{\omega_0} \approx -\frac{\Delta L}{2L}. \tag{73}$$

In order to substitute ΔL with σ_L, we have to take into account that a fluctuation of ω_0 leads always to a reduction of $|H(\omega)|$ close to its maximum because $|H(\omega)|$ is symmetric, and we have to scale the $\Delta\omega$ dependent term by approximately 0.5 in the numerator of Eq. (70). Using these relations, we finally obtain

$$\sigma_H = \left|\frac{\partial|H|}{\partial L}\right|\sigma_L \approx \frac{\frac{\sigma_L}{L}+\frac{1}{Q^2}}{2L\left(\left(\frac{\sigma_L}{L}\right)^2+\frac{1}{Q^2}\right)^{3/2}}\sigma_L \approx \frac{Q^3\Delta L}{2L^2}\sigma_L, \tag{74}$$

$$\sigma_\alpha = \left|\frac{\partial\alpha}{\partial L}\right|\sigma_L \approx \frac{Q}{L\left[1+\left(\frac{Q\sigma_L}{L}\right)^2\right]}\sigma_L. \tag{75}$$

The second approximation in Eq. (74) is only valid for very small σ_L. Furthermore, in these equations we assumed that Q is independent of σ_L, which gives valid results because in first order $\langle Q\rangle$ is independent of σ_L and Q does not depend on ω. If the circuit would be extended to allow for impedance matching, this simplification would not be valid anymore.

Although the situation of a serial LCR circuit is highly artificial for NMR probe circuits, the study of real circuits can be done in a similar way by modeling a circuit and comparing a numerical or analytical noise analysis to measured data. This can help identifying the primary source of vibrational noise in a probe, which can be used to design a setup with a reduced sensitivity to vibrations. For example, the strong Q-dependence of Eq. (74) suggests that stability problems which cannot be fixed easily, like with mobile samples as in medical imaging of in flow experiments, overcoupling of the resonant circuit may reduce noise considerably.

FLOW FLUCTUATIONS WITH REMOTE DETECTION

Remote detection NMR inherently employs a flowing fluid that transports information about an encoding environment to a separate detector. The encoding step modifies the longitudinal magnetization of nuclear spins contained in the fluid, and during detection this magnetization is read out as the fluid flows through the detector. To resolve the flow pattern of the encoded fluid to the detector as a function of time, t_{TOF}, after the encoding step, the detection volume must be smaller than the encoding volume. Detection is then done by applying a train of $\pi/2$ pulses with a fixed interpulse delay, Δt_{TOF}, starting right after the end of the encoding sequence [21]. For each of the detection pulses, the signal amplitude corresponds to one point in the TOF curve. The signal is at a maximum, S_0, if only unencoded fluid is in the detection volume, and the signal reduction from this maximum value is proportional to the number of encoded spins that are detected. The signal is further reduced if not all of the fluid in the detection volume is replaced between subsequent detection pulses. In an experiment where the encoding steps consists of a uniform excitation of the spin magnetization with a hard pulse of flip angle β_e, the signal can be modeled by

$$S(t_{\mathrm{TOF}}) = S_0 \frac{Q_v}{V_{\mathrm{d}}} \int_{t_{\mathrm{TOF}}-\Delta t_{\mathrm{TOF}}}^{t_{\mathrm{TOF}}} 1-(1-\cos(\beta_{\mathrm{e}}))P_S(t)\mathrm{d}t \tag{76}$$

$$\approx S_0 \frac{\Delta t_{\mathrm{TOF}} Q_v}{V_{\mathrm{d}}} \left(1-(1-\cos(\beta_{\mathrm{e}}))P_S\left(t_{\mathrm{TOF}}-\frac{\Delta t_{\mathrm{TOF}}}{2}\right)\right), \tag{77}$$

where $P_S(t)$ is the fraction of encoded spins that reach the detector at time t, Q_v is the volumetric flow rate of the fluid, and V_{d} is the detection volume. The approximation is valid if Δt_{TOF} is small enough that $P_S(t)$ can be assumed to be linear between two detection pulses. This equation assumes that no spins pass

the detection volume without being read out. Since in general the velocity of the fluid molecules cannot be considered as being uniform in the detection volume, this requires that Δt_{TOF} is shorter than theoretically required to replace all the fluid in the detection volume, *i.e.* $\Delta t_{\mathrm{TOF}} Q_v / V_{\mathrm{d}} < 1$.

The quantity that is most likely to fluctuate in such a flow system is Q_v. If we assume that these fluctuations are small enough not to affect the flow properties of the fluid, they primarily cause $P_S(t)$ to be stretched or compressed, while otherwise keeping its functional form. If we further suppose that Q_v changes slowly on the time scale of one detected transient and is therefore constant during one TOF transient, we can assume that the measured signal can be described by scaling the boundaries of the integral in Eq. (76) by a factor $\rho_Q = Q_v / \langle Q_v \rangle$. Then one obtains

$$S(t_{\mathrm{TOF}}) = S_0 \frac{\langle Q_v \rangle}{V_{\mathrm{d}}} \int_{\rho_Q (t_{\mathrm{TOF}} - \Delta t_{\mathrm{TOF}})}^{\rho_Q t_{\mathrm{TOF}}} 1 - (1 - \cos(\beta_{\mathrm{e}})) P_S(t) \mathrm{d}t \tag{78}$$

$$\approx S_0 \frac{\rho_Q \Delta t_{\mathrm{TOF}} \langle Q_v \rangle}{V_{\mathrm{d}}} \left(1 - (1 - \cos(\beta_{\mathrm{e}})) P_S\left(\rho_Q \tilde{t}_{\mathrm{TOF}}\right)\right) , \tag{79}$$

where $\tilde{t}_{\mathrm{TOF}} = t_{\mathrm{TOF}} - \Delta t_{\mathrm{TOF}}/2$. The differential signal change as a function of Q_v, which is needed for the error estimation, is

$$\frac{\partial S(t_{\mathrm{TOF}})}{\partial \rho_Q} = \frac{S(t_{\mathrm{TOF}})}{\rho_Q} - S_0 \frac{\rho_Q \Delta t_{\mathrm{TOF}} \langle Q_v \rangle}{V_{\mathrm{d}}} \tilde{t}_{\mathrm{TOF}} (1 - \cos(\beta_{\mathrm{e}})) \frac{\partial P_S\left(\rho_Q \tilde{t}_{\mathrm{TOF}}\right)}{\partial (\rho_Q \tilde{t}_{\mathrm{TOF}})} . \tag{80}$$

By using

$$\frac{\partial S(t_{\mathrm{TOF}})}{\partial t_{\mathrm{TOF}}} = -S_0 \frac{\rho_Q^2 \Delta t_{\mathrm{TOF}} \langle Q_v \rangle}{V_{\mathrm{d}}} (1 - \cos(\beta_{\mathrm{e}})) \frac{\partial P_S\left(\rho_Q \tilde{t}_{\mathrm{TOF}}\right)}{\partial (\rho_Q \tilde{t}_{\mathrm{TOF}})} , \tag{81}$$

we can estimate the multiplicative noise standard deviation from the standard deviation σ_{Q_v} of the flow rate as

$$\sigma_M(t_{\mathrm{TOF}}) = \frac{\partial \langle S(t_{\mathrm{TOF}}) \rangle}{\partial Q_v} \sigma_{Q_v} = \left[\langle S(t_{\mathrm{TOF}}) \rangle + \tilde{t}_{\mathrm{TOF}} \frac{\partial \langle S(t_{\mathrm{TOF}}) \rangle}{\partial t_{\mathrm{TOF}}} \right] \frac{\sigma_{Q_v}}{\langle Q_v \rangle} . \tag{82}$$

This equation states that we do not need to know the exact functional form of $P_S(t_{\mathrm{TOF}})$ to connect $\sigma_M(t_{\mathrm{TOF}})$ and σ_{Q_v}. It is sufficient to know the mean value of the signal and its first derivative with respect to t_{TOF}, which can be determined numerically from an experimental data set. Note that $\sigma_{Q_v} / \langle Q_v \rangle$ is simply the dimensionless relative flow rate standard deviation

A remote flow experiment as described above was performed on the 7.05 T magnet using a home-built probe with two saddle coils. The encoding volume was about 10 cm^3, and the detection volume was 0.7 cm^3.

Hyperpolarized ^{129}Xe in a gas mixture containing Xe:N_2:He=1:10:89 was used as the target nucleus. During encoding the spin magnetization was inverted with a hard on-resonant π pulse, and detection was done with a series of 40 $\pi/2$ pulses, spaced by 15 ms [37]. The FID after each of these pulses was multiplied with an exponentially decaying apodization function with a time constant of 0.5 ms. The additive noise level was $\sigma_+/S_0^{'} = 0.009$, where $S_0^{'} = S_0 \Delta t_{\mathrm{TOF}} \langle Q_v \rangle / V_{\mathrm{d}}$ is the signal amplitude when only unencoded gas was detected. Multiplicative noise due to B_0 fluctuations during each FID could not be detected due to the short detection time, and multiplicative noise caused by fluctuations of the pulse amplitude and phase was below the additive noise level.

The signal and its standard deviation of a gas flow experiment with remote detection is shown in Fig. 11. The fitted curve using Eq. (82) was obtained with $\sigma_{Q_v}/\langle Q_v \rangle = 0.036$. This result shows that a stable flow is of utmost importance with remote detection, especially if the TOF is resolved. The longer the distance between the encoding and the detection volume, the bigger the error that accumulates.

DISCUSSION AND CONCLUSIONS

Instrumental and experimental imperfections lead to noise of the spin magnetization of a sample that changes the relative value of the signal. This multiplicative noise increases during the course of an experiment from the moment the spin magnetization is excited out of its equilibrium state. The spectrum of multiplicative noise shows the same features as the spectrum of the signal, because each copy of the noise spectrum is offset by the same frequency as the lines themselves.

The phase of transverse magnetization is highly sensitive to very small fluctuations of B_0, which can have a significant impact not only with resistive [38], but also with superconducting magnets. These fluctuations can be spatially inhomogeneous, but are spectrally homogeneous, as every spin in a molecule experiences the same B_0 field. Especially susceptible are nuclei with a high γ, because the higher the precession frequency, the bigger the phase error that accumulates. Also multiple quantum experiments and experiments where the signal builds up over a long time during detection [11, 39] are more sensitive. A field–frequency lock, which corrects for drifts and very slow fluctuations of the resonance frequency, can be used to successfully reduce this phase noise as long as it is spatially homogeneous. Spatially inhomogeneous noise, which is created for

example by shim and gradient coils and their power supplies, is particularly severe because it cannot be corrected by a lock.

The power spectrum of B_0 noise depends on the spectrometer and its environment as well as the response of the field–frequency lock. It is not possible to give a generally valid expression for this noise contribution. Since the phase error that adds during free precession depends on the time integral of the B_0 noise, the power spectrum of the added noise scales with $1/f^2$ compared to the source noise power spectrum, therefore low-frequency noise contributes stronger to the measured signal than high-frequency noise. One simple model to describe B_0 noise, which takes advantage of this reduced influence of high-frequency noise, is to use an exponentially decaying autocorrelation function and a correlation time τ_B for the source noise. If τ_B is long compared to the echo time, it may be possible to at least partly refocus the effect of B_0 noise in an echo experiment.

Along the indirect dimensions in a multidimensional NMR experiment, multiplicative noise is basically white, and its impact is more obvious than in the direct dimension, where the noise spectrum has a width on the order or below the line width of the NMR signal and does not affect off-resonant spectral components. A common exception are sidebands due to line frequency harmonics. Because the width of the multiplicative noise spectral density is considerably smaller than the typical bandwidth of an NMR spectrum, oversampling in the direct dimension does not influence the sensitivity. In the indirect dimensions, oversampling has an equivalent effect as signal averaging, but certain types of artifacts like undesired signals along F_1 that normally would be aliased can simply be rejected [40].

If multiplicative noise is sensitivity limiting, increasing the signal by using a more concentrated sample does not improve the SNR. But it can be beneficial to increase the concentration of the nucleus used for field–frequency locking to get a more stable lock. In 2D experiments where the desired information is contained redundantly in symmetric locations with respect to the diagonal peaks, spectra can be symmetrized by comparing the signal intensities in each pair of symmetry-related locations and inserting the smaller of the two values into both locations [41]. This is especially successful if one of the two correlated peaks is covered by a stronger peak. Then the two cross-peaks are affected unequally by multiplicative noise, and only the weakly affected of the two is retained.

To avoid inheritance of noise between subsequent repetitions of an experiment, the recycle delay must be

long enough to allow relaxation of the magnetization sufficiently close to its equilibrium value. But increasing the length of the recycle delay more than necessary typically enlarges the multiplicative noise level due to an increased responsiveness to very low frequency changes of the noise-inducing process.

For experiments with a flowing fluid, fluctuations of the flow rate are an additional source of signal irreproducibilities. In remote experiments without TOF detection, flow errors can be somewhat reduced by increasing the detection volume above the volume of the encoded fluid such that all the encoded fluid is detected in a single step. If an experiment with TOF detection is done that requires more than one encoding step, the quality of the encoded information is degraded by a low flow stability. If the fluctuations of t_{TOF} increase above Δt_{TOF}, a reliable correlation between the encoded information and t_{TOF} is only possible if at the same time the fluid dispersion increases accordingly. Adjusting Δt_{TOF} using a moving average would then be a legitimate technique to increase the sensitivity at the expense of a reduced temporal resolution.

A possible workaround for multiplicative noise caused by mechanical instabilities of the rf circuits or problems with their grounding is to reduce the quality factor of the detection circuit by overcoupling [42], which causes a less steep transfer function of the circuit, but also reduces the signal. This approach can also be useful when two different fluids are mixed during an experiment [43].

During data analysis, one possibility to minimize multiplicative noise is to find an optimized filter function, which has to take into account the relative weight of the different noise contributions. Such an optimization could be done by reducing the spectral resolution in the direct dimension. However, if the resolution is reduced below the value given by a matched filter [2], this optimization competes with a decrease of the additive noise limited sensitivity. In the indirect dimension, non-transient multiplicative noise gets increased by a reduction of the time constant τ_1, while noise that accumulates during each t_1 evolution period gets reduced by a shorter τ_1. Therefore along t_1 it is usually preferred to reduce the resolution by keeping $t_1^{\max}$ as short as possible [44]. A general expression for the overall effect of reducing $t_1^{\max}$ depends on the pulse sequence and its timing, especially the ratio between $t_1^{\max}$ and the total length of the pulse sequence.

Because each spin of a particular nucleus experiences the same environmental noise, reference deconvolution along the direct dimension of a spectrum works particularly well to remove multiplicative noise [45, 46, 47]. Note that if such a reference deconvolution is implemented properly, which requires a well-resolved reference signal, multiplicative noise can be reduced by up to two orders of magnitude [46]. With

an optimized apodization as mentioned in the last paragraph, this improvement is considerably smaller and requires additionally to compromise on the resolution.

If some intrinsic knowledge about the data allows to reduce multiplicative noise during data processing, for example if it is known for a certain experiment that the noise behaves primarily according to either Eq. (47) or Eq. (48), it is advisable not to perform phase cycles during the acquisition, but to record and process every trace separately and do the phase cycling afterwards. This also allows, if necessary, to do a phase correction or a reference deconvolution on each recorded transient signal individually.

Apart from instrumental improvements and data analysis, there are also some possibilities and tools to reduce multiplicative noise on the level of the experiment design. In general, any method to remove unwanted signal components instead of subtracting them out improves the sensitivity. Instead of phase cycles, field gradients can be used as coherence pathway filters [9, 10]. This removes the noise accumulated on the dephased coherences, while a phase cycle retains multiplicative noise. Another possible technique is to use selective pulses [11]. Because multiplicative noise is proportional to the signal, weak signals can be buried in the noise of strong signals. If the strong signals can be selectively suppressed, the weak signals might be recovered.

The list of possible sources for multiplicative noise covered in this article is by no means complete. It depends on the experiment as well as on the spectrometer and its environment. In any case, knowing the dominant noise source is crucial, and a very important first step is to repetitively perform some simple experiments, where each is sensitive to a particular form of multiplicative noise. Repeating the same experiment with different probes, spectrometers, transmitter or receiver channels, samples, nuclei, or experimental parameters can help to distinguish between ordinary and defective behavior. And by knowing the origin and impact of multiplicative noise, it may be possible to eliminate its source, or at least to design techniques that are specific to a certain problem.

ACKNOWLEDGMENTS

I am grateful to Alex Pines for encouraging this work and for stimulating and helpful discussions. I would like to thank Julie Seeley, Andreas Trabesinger, Rachel Martin, Louis Bouchard, Jeffry Urban, Jamie Walls,

Dimitris Sakellariou, and Song-I Han for helpful discussions and their suggestions on the manuscript. This work was supported by the Swiss National Science Foundation through a postdoctoral fellowship, and by the Director, Office of Science, Office of Basic Energy Sciences, Materials Sciences of the US Department of Energy under Contract No. DE-AC03-76SF00098.

References

[1] Abragam A.: Principles of Nuclear Magnetism. Oxford: Oxford University Press 1961.

[2] Ernst R.R., Bodenhausen G., Wokaun A.: Principles of Nuclear Magnetic Resonance in One and Two Dimensions. Oxford: Clarendon Press 1987.

[3] Freeman R.: A Handbook of Nuclear Magnetic Resonance, 2nd edn. Singapore: Longman 1997.

[4] Trabesinger A.H., McDermott R., Lee S.K., Mück M., Clarke J., Pines A.: J. Phys. Chem. A **108**, 957-963 (2004).

[5] Hoult D.I., Richards R.E.: J. Magn. Reson. **24**, 71-85 (1976).

[6] Hoult D.I., Lauterbur P.C.: J. Magn. Reson. **34**, 425-433 (1979).

[7] Mehlkopf A.F., Korbee D., Tiggelman T.A., Freeman R.: J. Magn. Reson. **58**, 315-323 (1984).

[8] Weitekamp D.P.: Adv. Magn. Reson. **11**, 111-274 (1983).

[9] Horne T.J., Morris G.A.: Magn. Reson. Chem. **35**, 680-686 (1997).

[10] Lin G., Liao X., Lin D., Zheng S., Chen Z., Wu Q.: J. Magn. Reson. **144**, 6-12 (2000).

[11] Granwehr J., Urban J.T., Trabesinger A.H., Pines A.: J. Magn. Reson. **176**, 125-139 (2005).

[12] Richarz R., Wüthrich K.: J. Magn. Reson. **30**, 147-150 (1978).

[13] Lin Y.Y., Lisitza N., Ahn S.D., Warren W.S.: Science **290**, 118-121 (2000).

[14] Luck H., Trepp C.: Cryog. **32**, 690-706 (1992).

[15] Morris G.A.: J. Magn. Reson. **78**, 281-291 (1988).

[16] Morris G.A.: J. Magn. Reson. **100**, 316-328 (1992).

[17] Fukushima E., Roeder S.B.W.: Experimental Pulse NMR. A Nuts and Bolts Approach. Reading: Addison-Wesley 1981.

[18] Mehring M., Waugh J.S.: Rev. Sci. Instrum. **43**, 649-653 (1972).

[19] Martin R.W., Zilm K.W.: J. Magn. Reson. **168**, 202-209 (2004).

[20] Verhulst A.S., Liivak O., Sherwood M.H., Chuang I.L.: J. Magn. Reson. **155**, 145-149 (2002).

[21] Granwehr J., Harel E., Han S., Garcia S., Pines A, Sen P.N., Song Y.-Q.: Phys. Rev. Lett. **95**, 075503 (2005).

[22] Augustine M.P.: Prog. Nucl. Magn. Reson. Spectrosc. **40**, 111-150 (2002).

[23] Price W.S.: Concepts. Magn. Reson. **10**, 197-237 (1998).

[24] McCoy M.A., Ernst R.R.: Chem. Phys. Lett. **159**, 587-593 (1989).

[25] Huang S.Y., Walls J.D., Wang Y., Warren W.S., Lin Y.Y.: J. Chem. Phys. **121**, 6105-6109 (2004).

[26] Bloch F.: Phys. Rev. **70**, 460-474 (1946).

[27] van Kempen N.G.: Phys. Rept. **24**, 171-228 (1976).

[28] He Q., Richter W., Vathyam S., Warren W.S.: J. Chem. Phys. **98**, 6779-6800 (1993).

[29] Gardiner C.W.: Handbook of Stochastic Methods for Physics, Chemistry and the Natural Sciences, 2nd edn. Berlin: Springer 1985.

[30] Uhlenbeck G.E., Ornstein L.S.: Phys. Rev. **36**, 823-841 (1930).

[31] Press W.H., Teukolsky S.A., Vetterling W.T., Flannery B.P.: Numerical Recipes in C, 2nd edn. Cambridge: Cambridge University Press 1992.

[32] Edzes H.T.: J. Magn. Reson. **86**, 293-303 (1990).

[33] Williams G.A., Gutowsky H.S.: Phys. Rev. **10**, 278-283 (1956).

[34] Borer M.W., Maple S.R.: J. Magn. Reson. **131**, 177-183 (1998).

[35] Murali N., Kumar A.: Chem. Phys. Lett. **128**, 58-61 (1986).

[36] Bodenhausen G., Kogler H., Ernst R.R.: J. Magn. Reson. **58**, 370-388 (1984).

[37] Granwehr J., Seeley J.: J. Magn. Reson. **179**, 280-289 (2006).

[38] Sigmund E.E., Calder E.S., Thomas G.W., Mitrović V.F., Bachmann H.N., Halperin W.P., Kuhns P.L., Reyes A.P.: J. Magn. Reson. **148**, 309-313 (2001).

[39] Bowtell R.: J. Magn. Reson. **100**, 1-17 (1992).

[40] Nuzillard J.M., Freeman R.: J. Magn. Reson. A **110**, 252-256 (1994).

[41] Baumann R., Wider G., Ernst R.R., Wüthrich K.: J. Magn. Reson. **44**, 402-406 (1981).

[42] Schnall M.D., Subramanian V.H., Leigh J.S.: J. Magn. Reson. **67**, 129-134 (1986).

[43] Han S., Garcia S., Lowery T.J., Ruiz E.J., Seeley J.A., Chavez L., King D.S., Wemmer D.E., Pines A.: Anal. Chem. **77**, 4008-4012 (2005).

[44] Levitt M.H., Bodenhausen G., Ernst R.R.: J. Magn. Reson. **58**, 462-472 (1984).

[45] Gibbs A., Morris G.A.: J. Magn. Reson. **91**, 77-83 (1991).

[46] Gibbs A., Morris G.A., Swanson A.G., Cowburn D.: J. Magn. Reson. A **101**, 351-356 (1993).

[47] Morris G.A.: J. Magn. Reson. **80**, 547-552 (1988).

Figure Captions

Fig. 1

Signal-to-noise ratio as a function of the signal in an experiment where both additive and multiplicative noise are significant. Note that in a spectrum obtained by transient detection of an FID and subsequent Fourier transform, this SNR characterizes the reproducibility of the signal in a series of experiments, not the ratio of the signal to the off-resonant noise.

Fig. 2

Time dependence of noise. ^{1}H and ^{31}P data was measured using a mixture of H_3PO_4 (85 %):D_2O (4:1). A series of 2000 identical FID's was recorded on the 300 MHz spectrometer. The recycle delay was set to $5T_1$ for both nuclei, and the field–frequency lock time constant was set to the default value of 48 s. (*dashed lines*) Data of ^{1}H. (*solid lines*) Data of ^{31}P. (*a*) σ_S without any corrections. (*b*) Standard deviation σ_M of multiplicative noise only, divided by the signal intensity. After about 0.3 s, the multiplicative noise of the ^{31}P data becomes negligible. The inset shows the ^{1}H data points close to the beginning of the acquisition. The gray line is a calculated noise curve considering B_n as the only noise source.

Fig. 3

Influence of the field–frequency lock on the noise. A series of 128 identical ^{1}H FID's was recorded at 300 MHz. σ_M was determined separately for each point in t_2 using Eq. (7). (*a*) Variation of the lock time constant τ_l. A sample of 1% H_2O in D_2O, doped with 0.1 g/l $GdCl_3$ was used. The lock power was adjusted so that the lock level was slightly below its maximum. (*b*) Variation of the lock power. $\tau_l = 48$ s. A mixture of H_3PO_4:D_2O (1:1) was used. The labels indicate the lock level.

Fig. 4

Influence of the recycle delay on the noise. A series of 128 identical ^{1}H FID's was recorded. σ_S was determined using Eq. (7). A sample of pentane, doped with chromium diacetylacetonate to reduce T_1 to approximately 0.3 s, was used. (*a*) Variation of the recycle delay without lock, recorded at 300 MHz. (*b*) Variation of the

recycle delay with and without lock, recorded at 700 MHz. The lock parameters were adjusted using the automatic lock function of the spectrometer.

Fig. 5

Dependence of $M_z(t_0)$ on the timing of a two-pulse sequence. (*a*) Pulse sequence used for the model calculation. A spoiler gradient pulse at the end of the detection period is used to randomize any remaining transverse magnetization. (*b*) Steady-state $M_z(t_0)$ after an infinite number of identical experiments as a function of t_1. Three curves are shown for different values of the recycle delay t_r, corresponding to $t_r/T_1 = 1$, 2.2, and 5. T_2 was set to 1 s, and $\omega/2\pi = 20$ Hz. (*c*) $M_z(t_0)$ as a function of the number p of identical experiments that were performed. For the first point, the system was assumed to be in equilibrium, *i.e.* $M_z^{(1)}(t_0) = M_0$. The two curves correspond to the first minimum in Fig. 5b at $t_1 = 25$ ms and to the maximum at $t_1 = 50$ ms for $t_r/T_1 = 2.2$.

Fig. 6

Influence of different noise sources on the signal. The left column shows the real part of the time-domain noise, the right column the real part of the frequency domain contribution. (*a*) Noiseless signal. Using this signal, different noise contributions were calculated, and the difference to this ideal signal is shown below for the various noise sources. (*b*) Additive noise. The noise is white and independent of the signal in the time as well as in the frequency domain. (*c*) Multiplicative noise that adds prior to detection in the direct dimension. This leads only to a scaling and/or a phase shift of the signal. (*d*) Multiplicative noise adding transiently during detection. Initially the signal rises due to an increase of the phase error, and it is finally damped by relaxation. The noise hardly affects any off-resonant spectral components. In a properly phased spectrum the real part of the noise is antisymmetric with respect to the signal. (*e*) Multiplicative noise along the t_1 dimension from rf pulses and free evolutions that are unchanged along the indirect dimension. It is assumed here that this noise contribution is primarily amplitude noise, thus $\mathcal{N}(-\omega) = \mathcal{N}^*(\omega)$, and the real part of the spectrum shows a symmetric behavior around the center of the line. However, this assumption is only justified if t_2 is very short. (*f*) Multiplicative noise adding in the indirect dimension during t_1. It is increasing with t_1 before it is damped by relaxation. But subsequent data points are uncorrelated, therefore

white noise is added in the frequency domain. Even though it is phase noise that accumulates, rf pulses applied after the t_1 evolution convert it into amplitude noise. The phase noise contribution is mainly from the t_2 evolution.

Fig. 7

Multiplicative noise at the beginning of an FID. A sample of 1% H_2O in D_2O, doped with 0.1 g/l $GdCl_3$ was used. 128 identical experiments were performed at 700 MHz, and the data set composed of the first point of each transient trace was Fourier transformed. The abscissa shows the absolute value of the experiment rate. In black are the positive, in gray the negative frequency components. (*a*) Real part of the noise spectrum. (*b*) Imaginary part of the noise spectrum.

Fig. 8

SNR of a H_2O:D_2O (1:1) sample, recorded at 300 MHz. The gray line shows the calculated curve with $\tau_2 = 0.2$ s, $\sigma_B = 0.47$ nT, $\psi_A(0) = 320$, and an additive noise limited sensitivity of $\psi_+ = 30000$. The noise sidebands of the main signal are caused by coherent noise sources and are primarily at overtones of 60 Hz. The arrow marks noise lines caused by a small fraction of isopropyl alcohol that was added to the sample.

Fig. 9

Multiplicative noise in the frequency domain, recorded at 700 MHz. A sample of 1% H_2O in D_2O, doped with 0.1 g/l $GdCl_3$ was used. (*a*) Spectrum of the sample. No zero filling or apodization was used to process the data. (*b,c*) Absolute value of certain data points in 100 repetitions of the same experiment. (*b*) The position of the data point corresponds to the positions of the tilted arrows in 9a, respectively. The respective frequencies are equidistant to the center of the line. (*c*) The two curves correspond to two adjacent data points in the base of the line, corresponding to the vertical arrow in 9a. The scale is expanded 10 times compared to 9b. (*d*) SNR for different τ_2 as a function of the frequency offset $\Delta\omega$. (*solid*) Unaltered data set, no filter. (*dashed*) Multiply the time domain data with an exponential decay with $\tau = 50$ ms. (*dash-dotted*) $\tau = 20$ ms. (*dotted*) $\tau = 10$ ms.

Fig. 10

Serial LCR circuit. (*a*) Schematic representation. (*b*) Magnitude of the transfer function with $Q = 150$. *(c)* Phase of the transfer function. The higher Q, the smaller is the bandwidth of the resonant circuit, and the faster α changes around ω_0. This explains the strong dependence of σ_H and σ_α on Q.

Fig. 11

Multiplicative noise in a remote flow experiment. The time-of-flight of gas between two different locations was measured by first inverting the spin magnetization of hyperpolarized ^{129}Xe in the encoding volume with a hard π pulse, and then using a second, smaller coil to measure the magnetization of the gas as it was leaving the encoding volume. (*a*) TOF curve, showing the signal as a function of the time between the inverting encoding pulse and the detection pulses. (*b*) Standard deviation of the noise, relative to $S_0^{'}$. The experimental data points ($\circ$) were obtained from a set of 100 identical experiments, and the line is a fit using Eq. (82) with $\sigma_{Q_v}/\langle Q_v \rangle = 0.036$ and an additive noise contribution of $\sigma_+/S_0^{'} = 0.009$.

Figure 1:

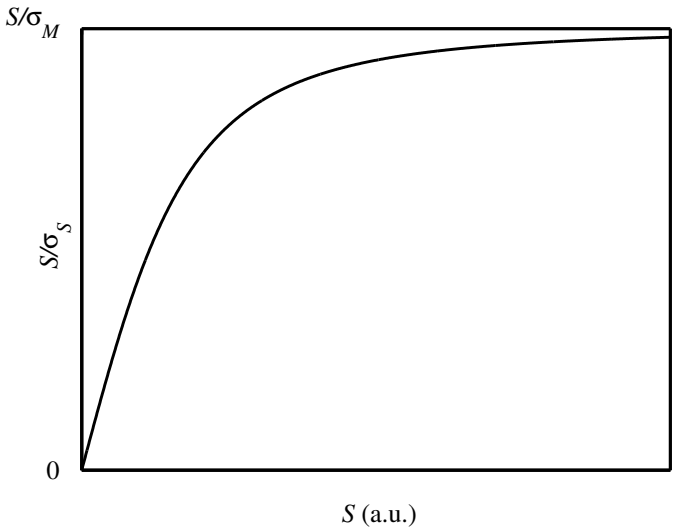

Figure 2:

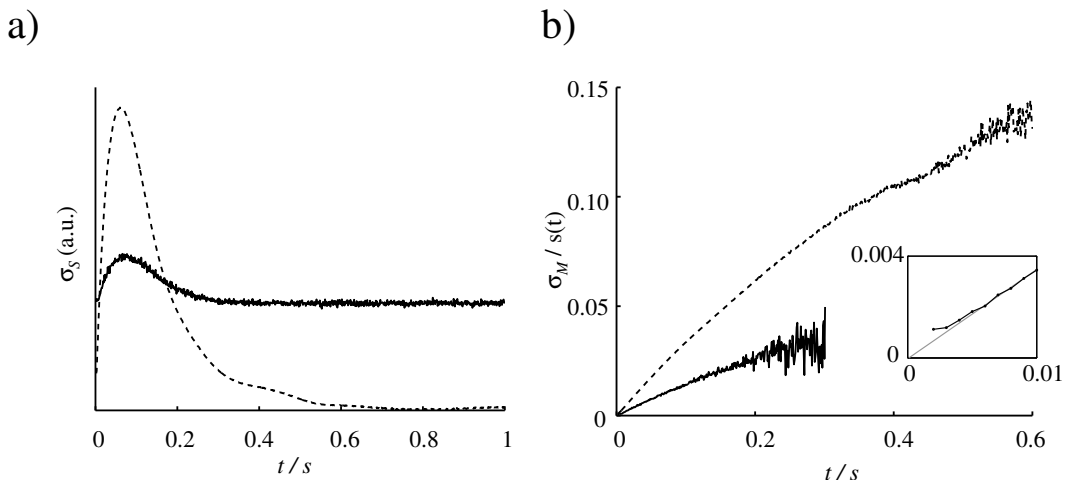

Figure 3:

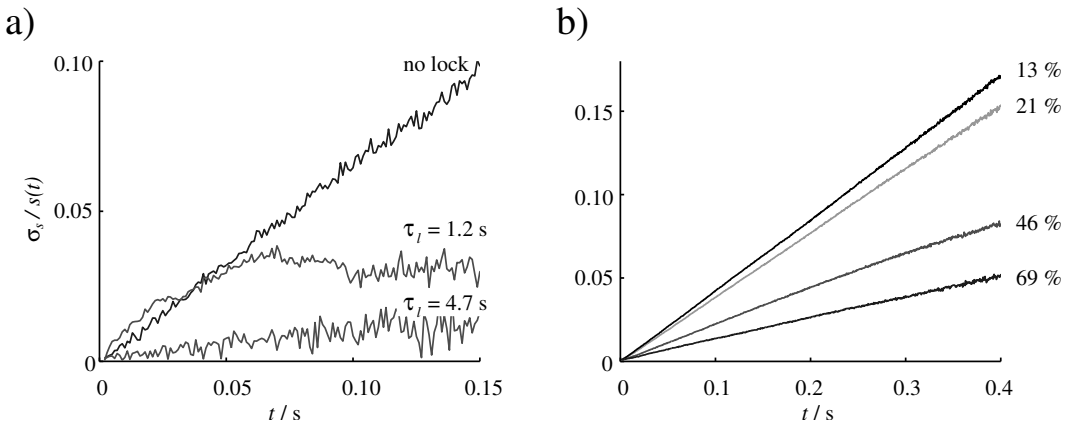
a)
b)
0.10
0.05
0
no lock
τ_l = 1.2 s
τ_l = 4.7 s
σ_s / s(t)
0
0.05
0.10
0.15
t / s
0.15
0.10
0.05
0
13 %
21 %
46 %
69 %
0
0.1
0.2
0.3
0.4
t / s

Figure 4:

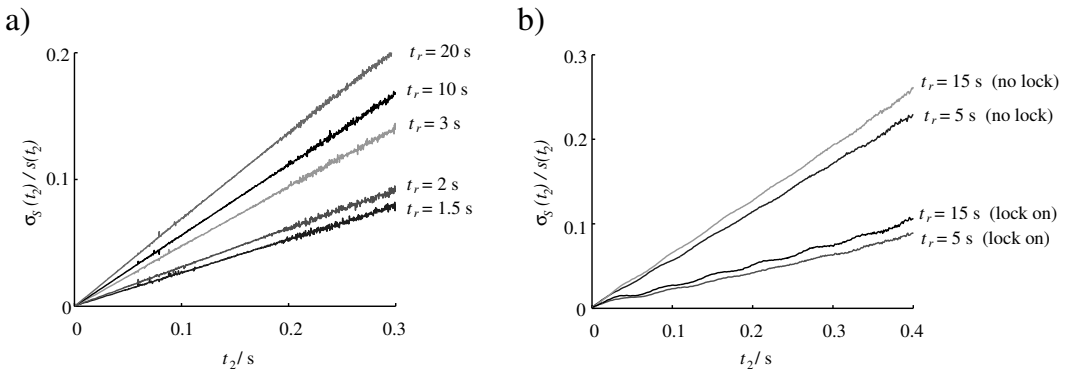
a)
b)
0.2
0.1
0
0.3
0.4
$\sigma_s(t_2)/s(t_2)$
t_2/ s
t_r = 20 s
t_r = 10 s
t_r = 3 s
t_r = 2 s
t_r = 1.5 s
t_r = 15 s (no lock)
t_r = 5 s (no lock)
t_r = 15 s (lock on)
t_r = 5 s (lock on)

Figure 5:

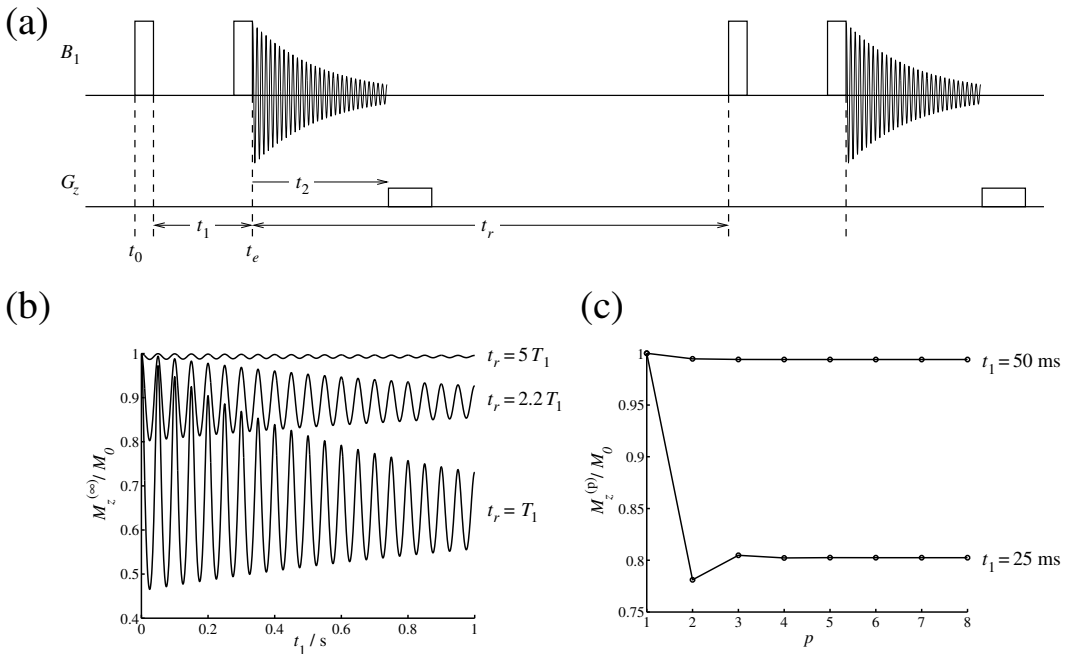
(a)
B_1
G_z
t_2
t_1
t_r
t_0
t_e
(b)
$t_r = 5\,T_1$
$t_r = 2.2\,T_1$
$t_r = T_1$
$M_z^{(\infty)} / M_0$
t_1 / s
(c)
$t_1 = 50$ ms
$t_1 = 25$ ms
$M_z^{(p)} / M_0$
p

Figure 6:

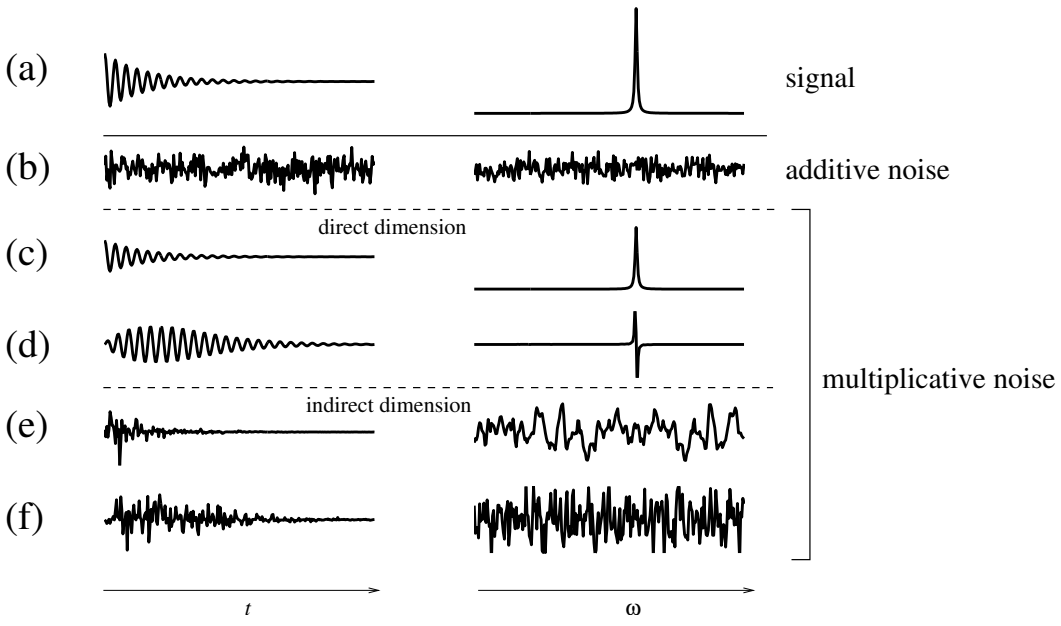
(a)
signal
(b)
additive noise
direct dimension
(c)
(d)
multiplicative noise
indirect dimension
(e)
(f)
t
ω

Figure 7:

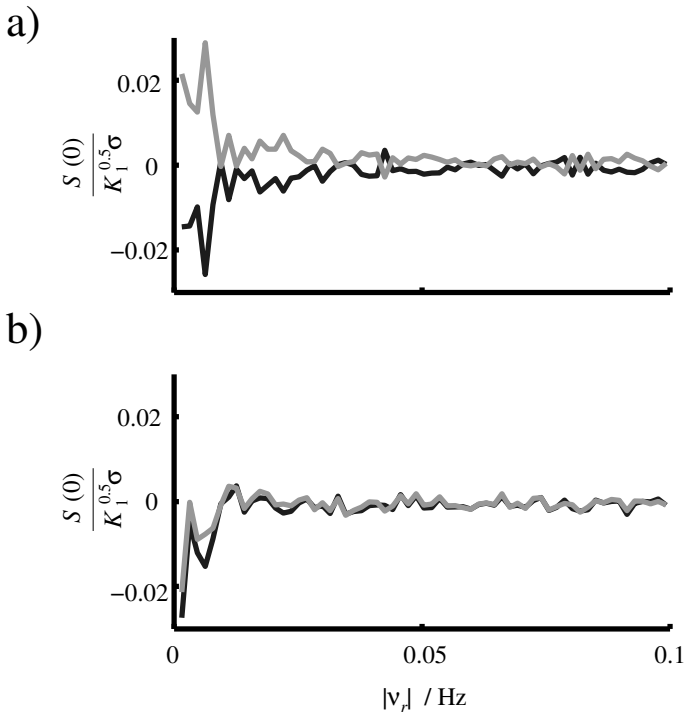
a)
0.02
0
−0.02
$\frac{S(0)}{K_1^{0.5}\sigma}$
b)
0.02
0
−0.02
$\frac{S(0)}{K_1^{0.5}\sigma}$
0
0.05
0.1
$|\nu_r|$ / Hz

Figure 8:

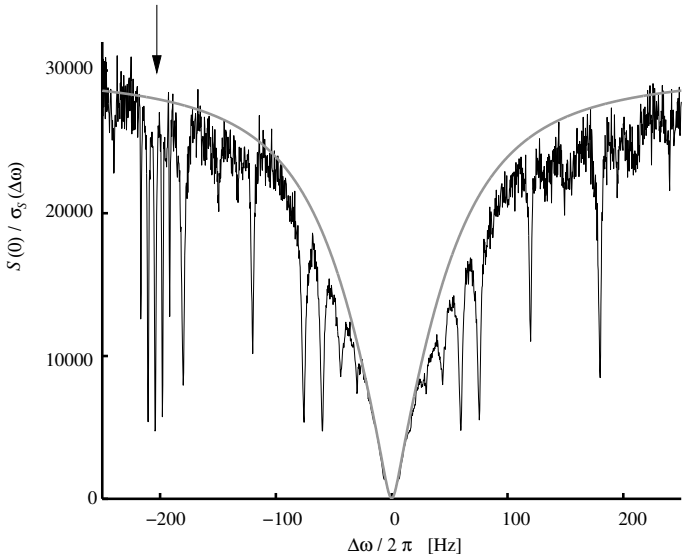

Figure 9:

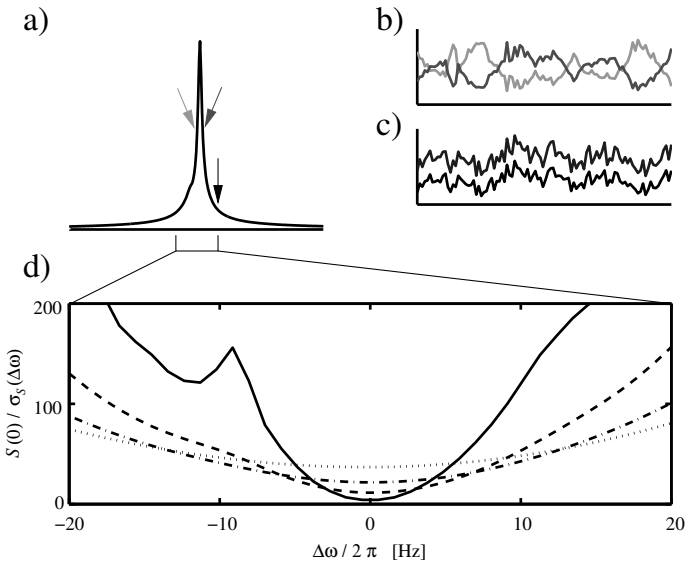

Figure 10:

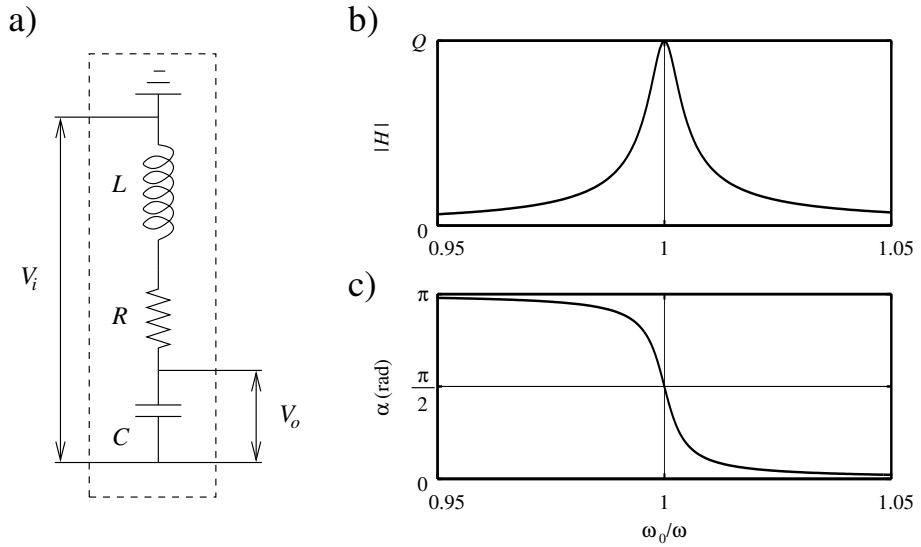

Figure 11:

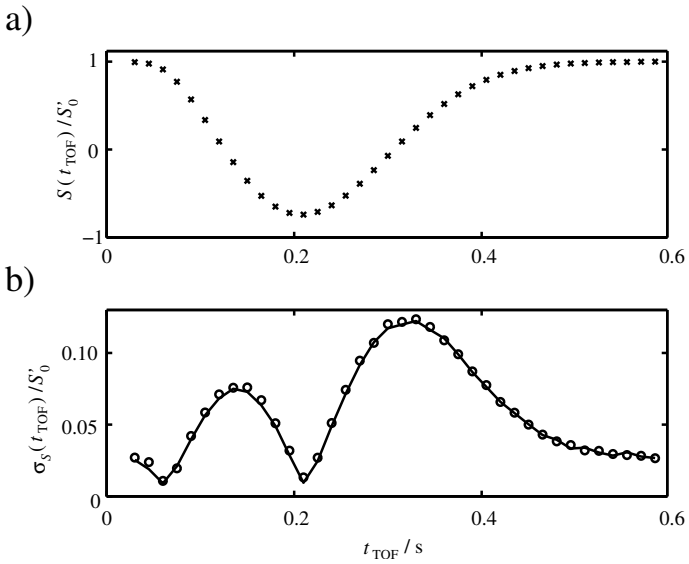
a)
1
0
−1
$S(t_{\mathrm{TOF}})/S_0'$
0
0.2
0.4
0.6
b)
0.10
0.05
0
$\sigma_S(t_{\mathrm{TOF}})/S_0'$
0
0.2
0.4
0.6
t_{TOF} / s